CHALMERS

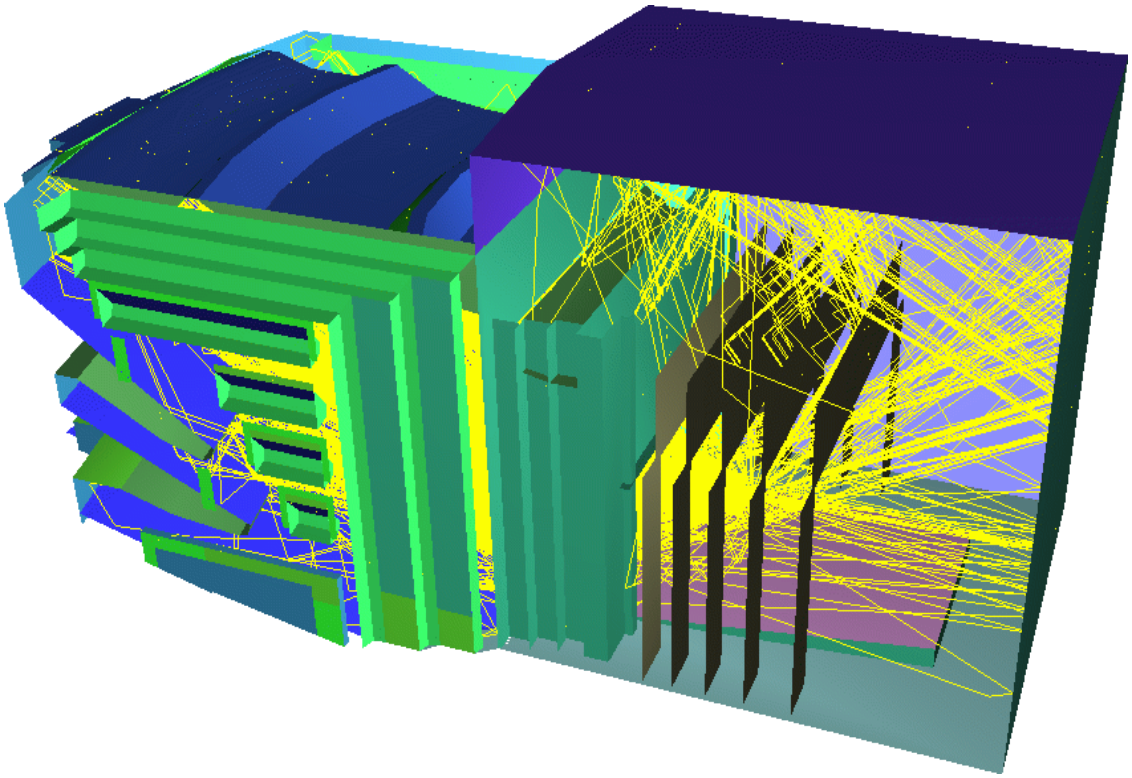

Limitations and improvements for a beam tracing simulation software applied to room acoustics

Master's Thesis in the Master's programme in Sound and Vibration

NICOLAS HERMANT

Department of Civil and Environmental Engineering
Division of Division of Applied Acoustics
Room Acoustics Group
CHALMERS UNIVERSITY OF TECHNOLOGY
Göteborg, Sweden 2010

Master's Thesis 2010:133

MASTER'S THESIS 2010:133

Limitations and improvements for a beam tracing simulation software applied to room acoustics

Master's Thesis in the Master's programme in Sound and Vibration

NICOLAS HERMANT

Department of Civil and Environmental Engineering
Division of Applied Acoustics
Room Acoustics Group
CHALMERS UNIVERSITY OF TECHNOLOGY

Göteborg, Sweden 2010

Limitations and improvements for a beam tracing simulation software applied to room acoustics
Master's Thesis in the Master's programme in Sound and Vibration
NICOLAS HERMANT

Master's Thesis 2010:133
Department of Civil and Environmental Engineering
Division of Applied Acoustics
Room Acoustics Group
Chalmers University of Technology
SE-412 96 Göteborg
Sweden
Telephone: + 46 (0)31-772 1000

Reproservice / Department of Civil and Environmental Engineering
Göteborg, Sweden 2010

Limitations and improvements for a beam tracing simulation software applied to room acoustics
Master's Thesis in the Master's programme in Sound and Vibration
NICOLAS HERMANT
Department of Civil and Environmental Engineering
Division of Applied Acoustics
Room Acoustics Group
Chalmers University of Technology

ABSTRACT

It has been investigated during the last decade that accurate modeling of diffuse reflection and diffraction is needed for room acoustic simulation and auralization. Limitations of the acoustic beam-tracing simulation software ICARE developed by C.S.T.B. have been studied, especially those due to the introduction of diffraction and diffusion for room acoustic simulations.

Until now the calculation of diffuse reflections was computed within ICARE using a statistical approach. This approach was using a white noise filtrated and temporally weighted according to Sabine's theory. It gave a global energetic estimation but its accuracy was not satisfactory compared to other room acoustic software. Therefore it has been decided to implement and to test a more precise model of diffuse reflections using an adapted particle tracing algorithm.

Presently few room acoustics software on the market takes into account the diffraction phenomenon which happens when the sound wave meets an edge or a curved surface. In rooms where the sound can be considered as almost always diffused - where the surfaces reflections are predominant and the distances between sources and receivers significant - the diffracted contribution in the simulation can be neglected. But, within rooms such as open offices where some surfaces have high absorption coefficients like the ceiling it could be assumed that diffraction phenomena cannot be neglected and could change the simulation results noticeably; even more if source and receiver are hidden one from each other. A study has been made on an actual case of a call center to see what difference was obtained with the inclusion of the diffraction phenomena.

Key words: room acoustics, diffusion, diffraction, simulation, particle, collector

Contents

Preface

This ten months Master thesis has been carried out from September 2009 to June 2010 within the room acoustics group of CSTB Grenoble, in France as an achievement of the Sound and Vibration Master program of Chalmers University of Technology, Sweden. This work focus on two room acoustics' phenomena modelling: the diffraction and the diffusion.

This work has been carried out with Isabelle Schmich, my supervisor at the CSTB, that I would like to thank for her great support during ten months. I would also like to thank Nicolas Noé, the developer of the ICARE software, Raphael Loyet, a PhD student at CSTB, for their great patience when explaining me all the room acoustics modelling concepts, for their help to conduct my calculation tests and to understand results sometimes quite strange. I would also like to thank Dirk Van Maercke, a researcher at CSTB, Christophe Rougier, an engineer at CSTB, Jérémy Rouch and Jan Jagla, two PhD students, for the interest they had for my thesis and the discussion we had to solve some issues.

Finally I would like to thank all the internship students, the PhD students, the researchers and all the employees that I have met at CSTB Grenoble during this ten months and who contributed to a really pleasant working atmosphere.

Grenoble, June 2010

Nicolas Hermant

Notations

α	Absorption coefficient
β_A	Splitting coefficient for the surface A
δ	Diffusion coefficient
$\bar{\delta}$	Mean diffusion coefficient
ρ_0	Density of the air
θ	Inclination angles between the normal of the reflection surface and the reflected trajectory
φ	Azimuth angles between the normal of the reflection surface and the reflected trajectory
Δ	Distance between the center of the collector and the particle's position in the collector
$\Delta\omega$	Solid angle
Ω	Opening angle of a beam
Θ	Inclinations angles for the definition of the truncated disc orientations
ϕ	Azimuth angles for the definition of the truncated disc orientations
Ψ	Angles used for the definition of the truncated disc area
c	Celerity of sound
e	Energy of the particles
h	Distance of the receptor or the source from a wall
n	Number of particles
p	Sound pressure
r	Distance covered by a particle
t	Time
z	Random number
A	Surface
C	Center of the receiver
G	Green's function
K	Ratio between the number of detected and emitted particles
N	Propagation order or reflection depth
N_f	Number of frequency bands
R	Radius of the collector
S	Source
V	Volume of a room
W	Sound power

1 C.S.T.B. and ICARE software

1.1 Room acoustics group at CSTB

CSTB (Centre Scientifique et Technique du Bâtiment in French) carries out research into a broad range of disciplines and technologies in every field of construction, including urban environment, health, communications, economics and sociology. The research furthers public policies and makes it possible to develop skills and showcase French engineering in major international projects.

In addition to carrying out the basic research required to improve fundamental knowledge, the research teams focus on structural themes and transversal projects. These themes highlight not only problems relating to risks and sustainable development, but also the tools and applications of information and communication technologies. They respond to trends in construction-related trades towards more management and renovation of real property, in particular via specific multi-disciplinary procedures [1].

During ten months, I have accomplished this thesis work within the room acoustics group which is one of the numerous groups of the Acoustic and Lighting department at CSTB. This group was composed of Isabelle Schmich, an engineer and the chief of this group; Nicolas Noé a researcher; Christophe Rougier an engineer; Paul Chervin a technician; Delphine Devallez a post PhD researcher and Jérémy Rouch a PhD student. The group activities are:

- **Consulting**: detailed acoustic studies for building projects like the National Grand Theatre of China (Beijing)
- **Research and Development**: acoustic simulation software, room acoustic active control …
- **Commercialization**, set up and adjustments of the CARMEN reverberation enhancement system.

1.2 ICARE software

ICARE is a software developed by CSTB for the acoustic propagation simulation based on asymptotic methods (ray theory). It models acoustic paths between sources and receivers with a hybrid method using beam tracing and ray tracing approaches. Originally intended at FRFs (Frequency Response Functions) narrow-band prediction for transportation industry it is now also used for room acoustics [2].

Initially the calculation of acoustic propagation for a room with ICARE was made following different steps which were the geometric calculation, the acoustic calculation and the post processing, as it is referred in Figure 1-1.

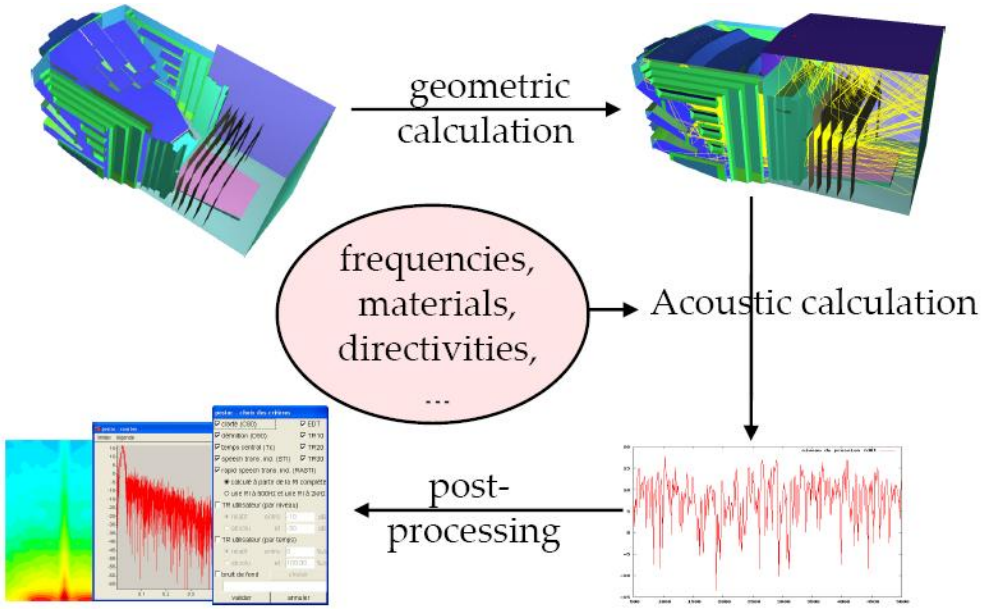

Figure 1-1: Different calculation steps within ICARE

1.2.1 Geometric calculation

The geometric calculation models exact propagation paths with respect to Fermat's principle between all the existing combination of sources and receivers. It models the specular and diffracted reflections on planar or curved surfaces using a beam tracing algorithm and the geometric theory of diffraction (GTD) [3].

The beam tracing method models the propagation of wave fronts represented with volumes, the beams, supported by three rays, c.f. Figure 1-2. Initially these volumes are pyramidal and stay like this until it intersects non-plane boundaries, for example curved surfaces. Once they intersect non-plane boundaries, they deviate from this pyramidal shape and the volume is determined by the geometry of the room and the three supported rays.

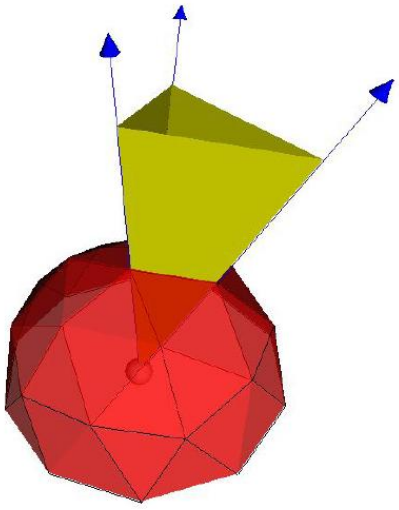

Figure 1-2: Initial subdivision of the solid angle around a source for the geometric tracing in [3]

Each beam needs to stay homogenous, i.e. it cannot contain any objects and each of the three supporting rays needs to have the same propagation history (intersect the same objects in the same order). Each non-homogeneous beam, or incoherent beam, is recursively subdivided into four new beams where the incoherence occurs, as can be observed in Figure 1-3.

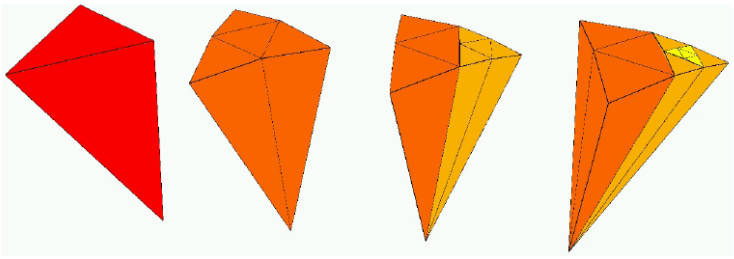

Figure 1-3: Adaptative beam subdivision in [3]

If a beam stays incoherent until a maximum subdivision value, the area where the incoherence occurs will be defined as a potential diffraction area, see Figure 1-4. Moreover if this area is defined in the geometry as a diffraction edge then an elementary interval is created on this edge. Therefore the set of inhomogeneous beams having the same history yields a set of elementary intervals referred to as a diffraction zone.

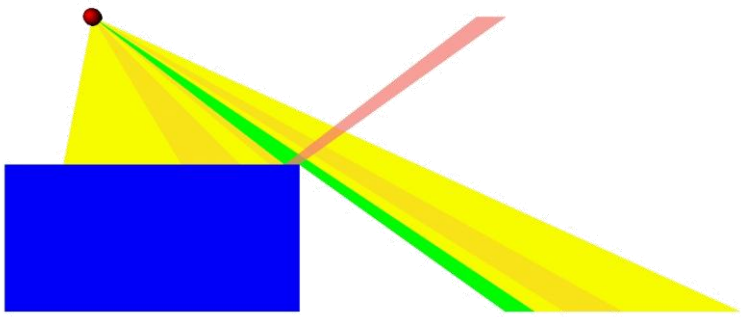

Figure 1-4: homogeneous beams (yellow) and non-homogeneous beam (green) in [3]

Each diffraction interval yields diffracted beams that are constructed according to the Uniform Theory of Diffraction [3]. Rather than originating from a point source, the diffracted beams originate from a section of the edge. Their volume is defined by Keller's cones at each end of the interval, and the associated wedge planes. The tracing algorithm, described earlier, is then applied to the new diffracted beams, now defined by four instead of three rays.

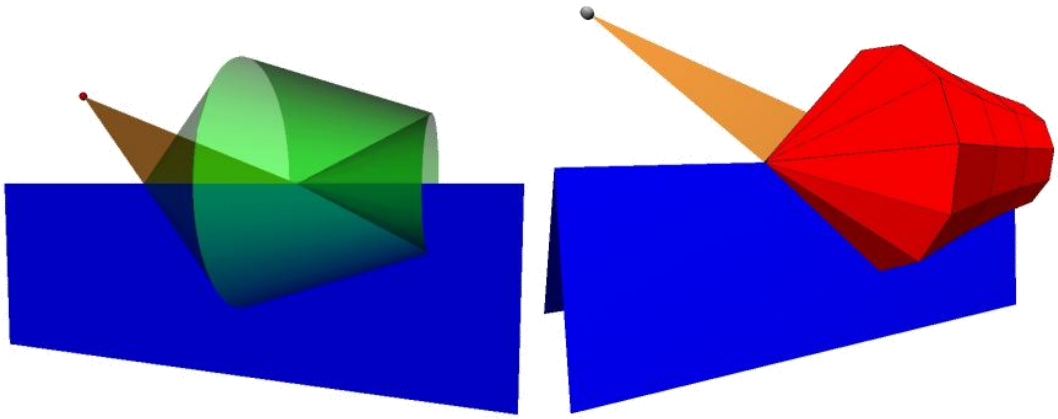

Figure 1-5: space of diffracted beams defined by Keller's cones (left) and the diffraction edge as a secondary source (right) in [3]

Once the beams have finished their propagation in the room, i.e. when the maximum reflection order has been reached, one wants to know if beam volumes contain a receiver and then one wants to calculate the exact path between the source and the receiver. These steps refer to point locating techniques, over estimation of the volumes and some other notions which description can be found in [3].

- **Some important parameters of geometric calculations:**

In ICARE one needs to define the following input parameters for the beam tracing calculations. These parameters values will define how the beams can propagate into the room.

- Maximum propagation depth (or reflection order): the number of reflections, (refractions in case of moving media) or diffractions encountered during tracing will not exceed this value
- Maximum number of diffraction that can be processed during a path
- Limitation of the reflection order on each side of the diffraction: limit the propagation order before and after each diffraction edge
- Paths only into the shadow area: creation of diffraction edges that only generate paths in the shadow area of these edges

1.2.2 Acoustic calculation

For this calculation the user needs to define the following parameters:

- The temperature that will define the celerity of sound
- The relative humidity of the air which is used to compute the air absorption

- The frequency range
- The material properties: absorption and diffusion coefficient for each octave bands
- Directivities, power of sources and/or receivers

Green's function is calculated for each path, see [3].

2 Modelling diffuse reflections using an adapted particle tracing algorithm

Until now the calculation of diffuse reflections was computed within ICARE using a statistical approach [4]. The same approach used to compute the late part of the impulse response.

This statistical approach is using a white noise filtrated and temporally weighted according to Sabine's or Eyring's formula. It gives a global energetic model but its accuracy is not satisfactory whereas it has been shown during the last decade that an accurate modelling of diffuse reflection is needed for room acoustic simulation and auralization [10] [15] [16]. According to that it has been decided to implement a more precise model of diffuse reflections using an adapted particle tracing and to combine it with the CSTB beam tracing algorithm. This combination will result in a hybrid model that is able to handle specular and diffuse reflections for a good estimation of the early and late part of the impulse response.

ICARE initially offered an existing basic particle tracing algorithm that was used few years ago for a study on acoustic diffusion functions (BRDFs). It allowed simulation of any kind of diffuse and specular reflection but was disconnected from the beam-tracing algorithm, primitive and not user-friendly.

The particle tracing is a Monte Carlo method used to solve the integral forms of sound propagation [5]. The Monte Carlo's concepts were used, at the beginning of computer era, by Allred and Newhouse to model architectural acoustics, [6] and [7]. The Monte Carlo integration methods provide solutions to evaluate definite integrals, particularly multidimensional integrals with complicated boundary conditions. They use randomness to estimate the values of integrals [8].

Furthermore for the particle tracing methods, particle detection using a receiver is an important problem. Detection problems caused by improper receivers lead to inexistent or diminished detection which distort the precision of the particle tracing calculation [10]. For this reason the modelling of the collector which detects particles has been a major axis of the algorithm development.

2.1 Particle tracing basics

Particle tracing is a simulation method which is very used in lighting numerical modelling because it is really convenient for simulating the behaviour of large number of particles. It is also a commonly used technique in acoustic simulation because it is a very flexible method which makes possible to model any reflection's law. Furthermore the basic particle tracing algorithm is quite easy to implement in an existing ray-tracing environment.

During a particle tracing the source is emitting Dirac impulses in random directions. Each particle propagates at the celerity of sound with a certain amount of energy and bounds on the walls of the room. Each wall absorbs and reflects some of the particle's energy. At each reflection the sound can be divided in two parts: the specular reflection and the diffuse reflection, c.f. Figure 2-1. These two parts can be related using the absorption and diffusion coefficients α and δ with the following Equation (2-1):

$$(1-\alpha)(1-\delta)+\alpha+(1-\alpha)\delta=1 \qquad (2\text{-}1)$$

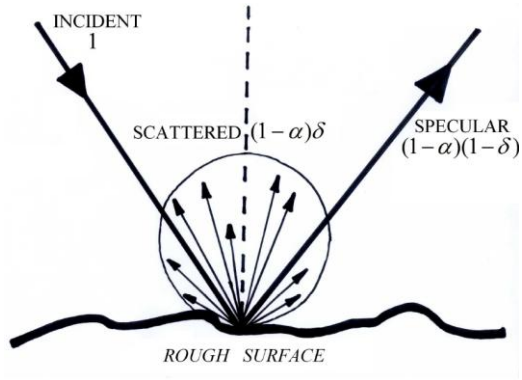

Figure 2-1: Particle's energy at a reflection

The absorption does not have any influence on the particle tracing modelling because it does not affect the trajectory of the particle. It will not be taken into account in the geometric calculation but only in the acoustic calculation which considers the acoustic properties of materials and the frequency dependency. On the other hand, diffusion is crucial when it comes to the particle's trajectory and it is a frequency dependent phenomenon.

There are several solutions to consider the diffusion within a particle tracing model. One is the attenuation of the incident energy weighting it by $(1-\alpha)(1-\delta)$ for the specularly reflected part and by $(1-\alpha)\delta$ for the diffusively reflected part. The particle is emitted with incident energy e_0 and propagates until a minimum energy is reached [13]. Another method consists in applying a stochastic attenuation to the particles by creating random numbers $(z_1, z_2) \in [0;1]$ and comparing them with the absorption coefficient α and the diffusion coefficient δ : if $z_1 < \alpha$ the particle is absorbed and if $z_2 < \delta$ the particle is diffused. If the particle is not diffused, it is specularly reflected; otherwise the particle emitted off a diffusing surface is distributed randomly using a Lambert distribution [19] [20] [30]. For our model, a stochastic approach has been used without annihilating the absorbed particles. This approach is described in details in the following Part 2.2.

2.2 Particle tracing within ICARE

This part describes what is happening to a particle emitted from a source, propagating into the room and detected by a particle tracing collector. The following concepts described in this part have been used in the new ICARE's algorithm.

2.2.1 Splitting coefficient

The source is randomly emitting n_{source} particles which will reflect on partially diffusing surfaces. For each reflection a random number z is created and is compared to a coefficient β_A called "splitting coefficient" by J.J. Embrechts in [15], which is defined for the surface A. If $Z \leq \beta_A$ then the reflection is diffuse otherwise it is specular. The particle energy can be described by the following Equation (2-2):

$$\langle \hat{p}_{sc}^2 \rangle = \frac{\delta_A(f)}{\beta_A} p_{diff}^2(\Delta S) + \frac{1 - \delta_A(f)}{1 - \beta_A} p_{spec}^2(\Delta S) \qquad (2\text{-}2)$$

Where:

$\delta_A(f)$ is the diffusion coefficient of surface A for the considered octave (or one-third octave) band;

ΔS is the receiver surface;

p_{diff} is the diffuse contribution of the sound pressure received at the detector;

p_{spec} is the specular contribution

Coefficient β_A can be defined by the mean value of all the diffusion coefficients of the diffuse surface over the frequency bands in order to avoid a possible amplification or attenuation of the diffused energy over the considered frequency band. On the other hand this definition of the splitting coefficient seems inappropriate when the diffusion coefficients are very distant within the different frequency bands. Indeed, it could result in a higher variance of the diffuse behaviour of the material but it should be compensated by the fact that a lot of particles are emitted during a particle tracing.

2.2.2 Number of particle received by the collector: probabilistic approach

The problem of the particles propagating in the room's space can be seen using a probabilistic approach [21]. The purpose of this part is to formulate the number of particles that will be detected by a collector (a disc in this part) when a source is emitting a certain number of particles.

Considering that at each time t a particle could be described in the 5 dimensions phase space:

- $p(x_i, y_i, z_i)$: the particle's current position
- $q(\theta_i, \varphi_i)$: the particle's direction of propagation

The assumption of the ergodic behavior of particles implies an uniform distribution in the phase space which leads to express the probability P for a single particle to be found in an elementary volume by the following Equation (2-3):

$$P = \frac{1}{V} \times \frac{1}{4\pi} \qquad (2\text{-}3)$$

Where V is the volume of the room.

If the source emits n_{source} particles then the number of particles dn in the elementary volume is:

$$dn = \frac{n_{source} \cdot dp \cdot dq}{4\pi V} \qquad (2\text{-}4)$$

Let us consider $n(t, t + \Delta t)$ the number of particles from visible image sources reaching the receiver in the interval $[t, t + \Delta t]$, an arrival will be detected if the particle is found in a region as described on the following figures:

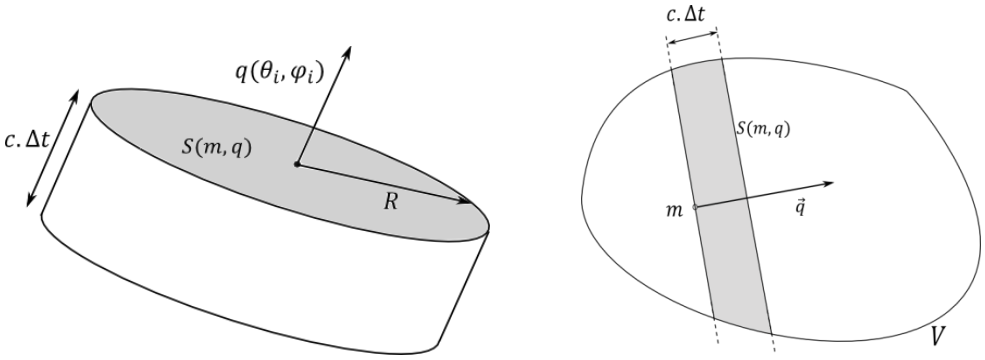

Figure 2-2: Elementary volume and orientation of the detection disc

This means that a particle will be detected if and only if $\begin{cases} (m - p_i) \cdot r_i > 0 \\ (m - p_i) \cdot r_i < c\Delta t \end{cases}$

Where:

m is the receiving position;

r_i is a vector of unitary length corresponding to the direction of propagation q_i.

The number of arrivals at the receiver from a given direction q is equal to the number of particles in the volume $S(m, q)c\Delta t$, which leads to the following equations:

$$dn = \frac{n_{source}}{4\pi V} S(m,q) c\Delta t \qquad (2\text{-}5)$$

Then for an elementary portion dS of $S(m,q)$ the number of arrivals will be

$$dn = \frac{n_{source}}{4\pi V} c\Delta t \cdot dS \qquad (2\text{-}6)$$

At a given time t the number of particles received by the detection disc is

$$n(t) = \int_{4\pi} \int_{S(m,q)} \frac{n_{source}}{4\pi V} c\Delta t \cdot dS = \frac{n_{source} c\pi R^2 \cdot 4\pi}{4\pi V} = \frac{n_{source} \pi R^2 c}{V} \qquad (2\text{-}7)$$

For an interval of time Δt the number of particles received by the disc is:

$$n(\Delta t) = \frac{n_{source} \pi R^2 c \Delta t}{V} \qquad (2\text{-}8)$$

2.2.3 Number of particle received by the collector: geometric approach

This part describes a different approach of the same problem: a geometric approach of the particle tracing. This geometric approach also tries to formulate the number of particles that will be detected by a collector when a source is emitting a certain number of particles. In this approach the collector is defined with a sphere but a particle is actually detected by the disc inside the sphere which normal is perpendicular with the particle's trajectory.

This geometric approach is done for specularly reflected and diffusively reflected particles.

- **Specular reflection**

The case of a simple specular reflection is represented in Figure 2-3: with S the source and S' the image source.

If a source S emits n_{source} particles in random directions then only a certain number n_{spec} will cross the sphere. The situation can be seen from the image source S' which is located at a distance r_{total} from the center *C* of the detection disc, i.e. the actual receiver position. Considering that the image source S' also emits n_{source} particles in random directions, only n_{spec} particles are in the solid angle $\Delta\omega$ which encompasses the sphere, which is equivalent to the following Equation (2-9):

$$n_{spec} = \frac{n_{source}}{4\pi} \Delta\omega \qquad (2\text{-}9)$$

This number also corresponds to the number of particles received in the detection disc, which area is $= \pi R^2$, inside the sphere which is perpendicular with the particle's trajectory, c.f. Figure 2-3, so one can write Equation (2-10):

$$\Delta\omega = \frac{A}{r_{total}^2} = \frac{\pi R^2}{r_{total}^2} \qquad (2\text{-}10)$$

The number of particles specularly reflected crossing the detection disc can be expressed with the Equation (2-11):

$$n_{spec} = \frac{n_{source}}{4} \times \frac{R^2}{r_{total}^2} \qquad (2\text{-}11)$$

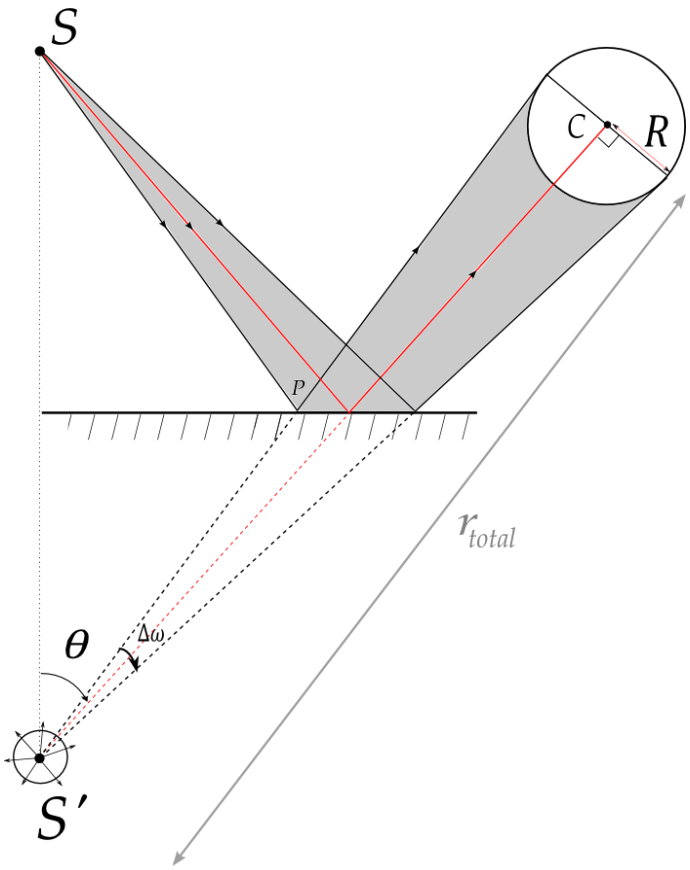

Figure 2-3: A specular reflection

- **Diffuse reflections**

Considering that the diffuse reflection must be randomly directed and with a projected solid angle. The following figure is a random draw of a particle after a diffuse reflection at the point P, see Figure 2-4.

The number $n_{diffuse}$ of particles diffused in $\Delta\omega$ can be expressed with the following Equation (2-12):

$$\frac{n_{diffuse}}{\Delta\omega \cos\theta} = \frac{n}{\int d\omega cos\theta} \qquad (2\text{-}12)$$

Where:

n particles are diffusively reflected from point P;

R is the radius of the detection disc;

$r_{partial}$ is the distance from the reflection point to the centre of the sphere;

$\Delta\omega$ is the solid angle;

θ is the angle between the normal of the reflection surface and the solid angle.

With $\int d\omega cos\theta = \int_0^{\pi/2} cos\theta sin\theta d\theta \int_0^{2\pi} d\varphi = \pi$

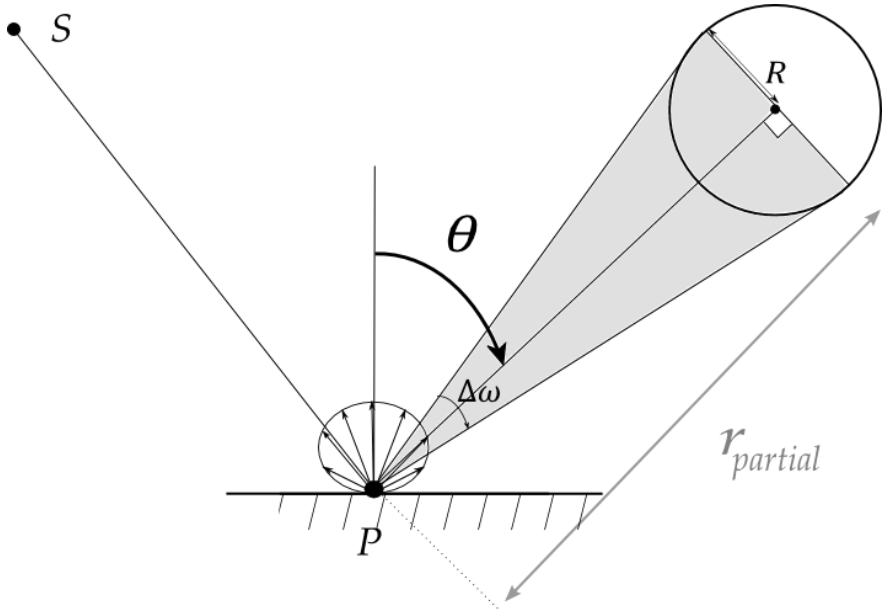

Figure 2-4 representation of a punctual diffuse reflection

Then Equation (2-12) becomes:

$$n_{diffuse} = \frac{n\Delta\omega \cos\theta}{\pi} = \frac{n}{\pi}\frac{Acos\theta}{r_{partial}^2} = \frac{n}{\pi}\frac{\pi R^2 cos\theta}{r_{partial}^2}$$

$$n_{diffuse} = \frac{nR^2}{r_{partial}^2} cos\theta \qquad (2\text{-}13)$$

Let us define the total number of (specular and diffuse) particles n_{sphere} received by the sphere when n_{source} particles are emitted by the source.

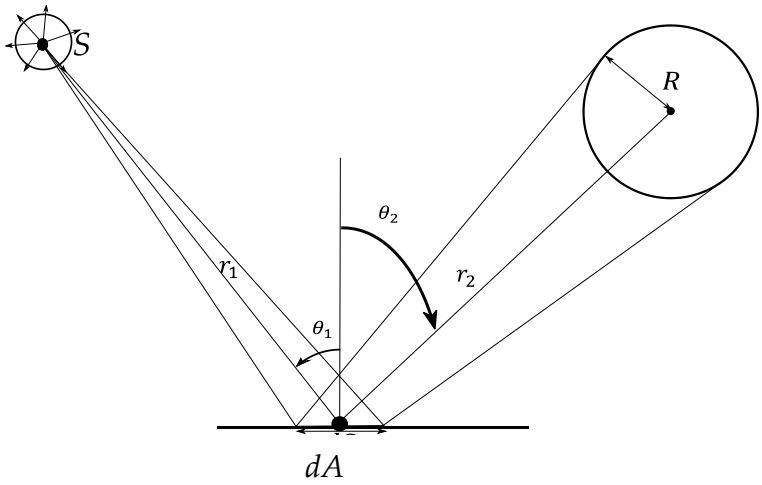

Figure 2-5: representation of a diffuse reflection on an elementary surface

We know that the number of particles $dn_{incident}$ arriving on a surface element dA as described in Figure 2-5 can be formulated with Equation (2-14):

$$dn_{incident} = \frac{dA cos\theta_1}{\pi r_1^2} \times n_{source} \qquad (2\text{-}14)$$

Where:

θ_1 is the angle between the normal of the surface and the trajectory of the incident particle;

$r_1$is the distance between the source and the reflexion point;

θ_2 is the angle between the normal of the surface and the trajectory of the reflected particle;

r_2 is the distance between the reflexion point and the centre of the collecting sphere, i.e. the position of the receiver.

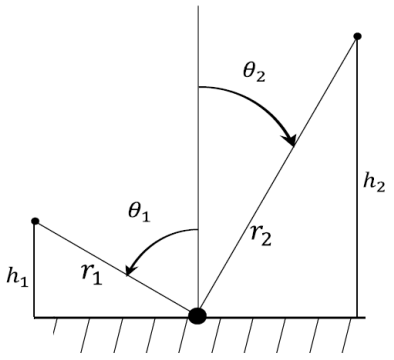

Figure 2-6: angles, distances and trajectories during a diffuse reflection

The number of diffused particles $n_{sphere,diffused}$ received by the sphere is equivalent to the sum on the surface dA of the punctual diffuse reflection described on Figure 2-4, thus $n_{sphere,diffused}$ can be expressed by Equation (2-15):

$$n_{sphere,diffused} = \int dn_{incident} \frac{R^2 cos\theta_2}{r_2^2} = R^2 \, n_{source} \int \frac{cos\theta_1 cos\theta_2 dA}{\pi r_1^2 r_2^2} \qquad (2\text{-}15)$$

In the particular case where the source and the receiver coincide ($r_1 = r_2 = h$) one can write Equation (2-16).

$$n_{sphere,diffused} = \frac{n_{source} R^2}{4h^2} \qquad (2\text{-}16)$$

In a general case the result of Equation (2-15) can be approximated with the following result:

$$n_{sphere,diffused} \cong \frac{n_{source} R^2}{4r_2^2} \qquad (2\text{-}17)$$

2.2.4 Variable radius of the detection disc

In a stochastic algorithm the smaller the detector is the weaker the probability is for the particle to cross the detector. To increase this probability one can increase the number of emitted particles which increases the calculation time or one can increase the size of the detector which decreases the spatial accuracy of the results.

When a particle crosses the detecting disc of a receiver, its energy is stored at a time $t = t_0 + \sqrt{(t_D - t_0)^2 + c^2.\Delta^2}$ within an echogram.

Where:

c is the speed of sound;

t_0 is the time for the particle to arrive at the reflection point P;

t_D is the time for the particle to arrive at point D in the detection disc, c.f. Figure 2-7.

The storing time t is the time that the particle would take to come from an image source position to the center of the detection disc, which is the real position of the receiver.

Figure 2-7 pictures a particle crossing the detection disc in point D at a time t_D; the blue line is the real path of the particle and the red line is the path if the particle would have arrived from the image source to the center of the receiver C, Δ is the distance between C and D.

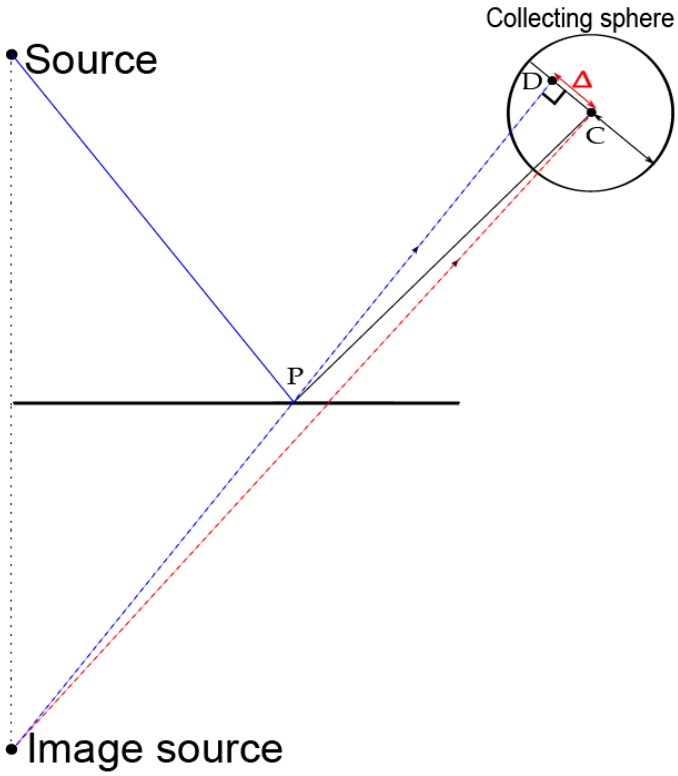

Figure 2-7: Particle crossing the detection disc

From this storage concept the particle tracing approach differs from the beam tracing one and could introduce some underestimation of the detected energy for some peculiar cases. Indeed the particle tracing approach is not an approach which considers the receiver as a point receiver like it is done in the beam tracing approach. As pictured in Figure 2-8, the particle tracing uses a sphere to collect the particles, and it could happen that some parts of this sphere exceed the reflected zone of an object. No particles can be detected in those exceeding parts, but the global energy of the particles detected by the collector is normalized using the complete area of the detection disc which leads to an underestimation of the global energy.

In order to minimize the errors which results from the cases represented in Figure 2-7 and Figure 2-8, it has been decided to investigate a parametric size of the collector. Moreover in [10], [15], and [16] it is shown that statistical errors could be minimized if one pays really attention to the choice of the number of rays and the size of the receiver. A changeable size collector should be really helpful to avoid systematic statistical error and even more if it is adapted to any receiver positions.

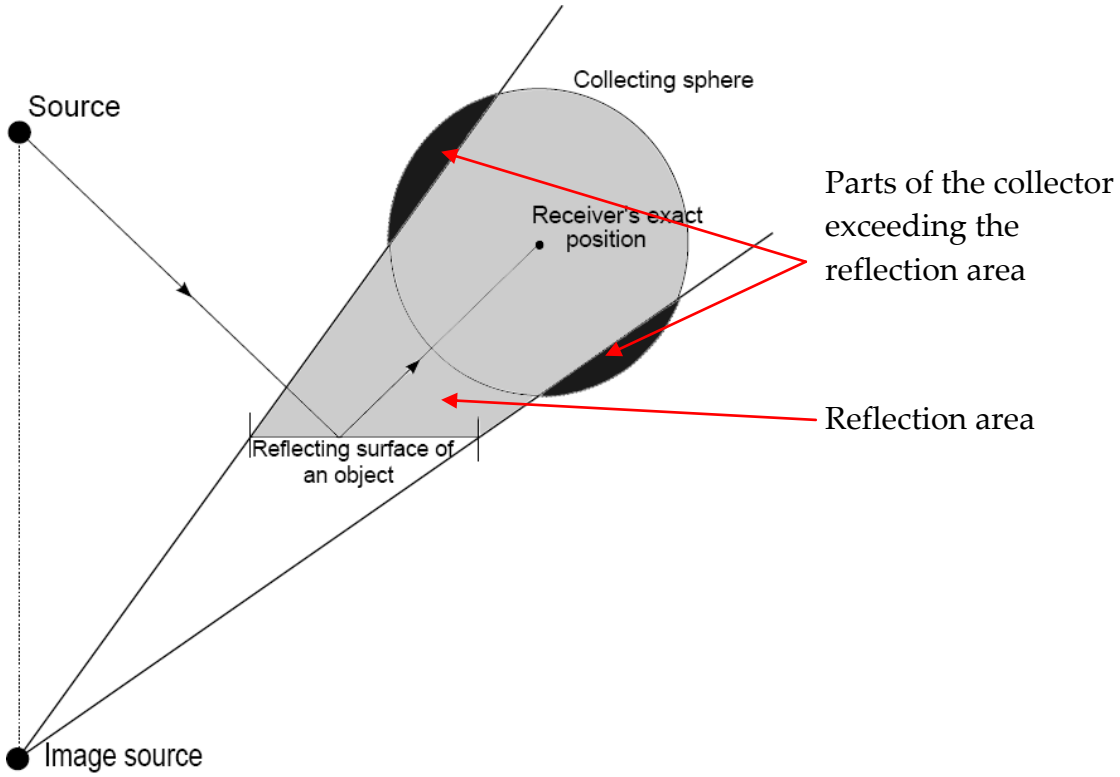

Figure 2-8: parts of the sphere exceeding from the reflection area

The following parts describe how to compute a size adaptive spherical collector.

- **Radius with the probabilistic approach**

According to Equation (2-8) the radius R of the detection disc can be expressed, with Equation (2-18):

$$R = \sqrt{\frac{K \cdot V}{\pi c \Delta t}} \qquad (2\text{-}18)$$

K is the ratio between the number of particle detected and the number of particle emitted. Then to make the sphere grow one needs to increase the ratio K with the propagation order. It could be done using a law or just by increasing values of K for increasing propagations orders.

- **Radius with the geometric approach**

Otherwise, as it has been seen in part 2.2.3 the number of diffused particles collected by the sphere can be approximated by Equation (2-17). Wherein $r_2 = r_{last}$ is the distance covered by the particle between the last reflection and the intersection with the surface within the sphere which is perpendicular with the

particle trajectory and which contains the centre of the collecting sphere, i.e. the detection disc.

In a similar way it is possible to obtain the number of specularly reflected particles collected by the sphere as

$$n_{sphere,specular} = \frac{n_{source}R^2}{4r_{total}^2} \qquad (2\text{-}19)$$

Wherein r_{total} is the total distance covered by the particle from the source to the centre C of the detection disc.

To obtain the total number of particles collected by the sphere, $n_{sphere,total}$ one needs to weight $n_{sphere,diffused}$ and $n_{sphere,specular}$ by the mean diffusion coefficient $\bar{\delta} = \sum_i \delta_i f_i$, where f_i is the impact frequency of particles on the material i with the diffusion coefficient δ_i.

$$n_{sphere,total} = (1 - \bar{\delta})n_{sphere,specular} + \bar{\delta}n_{sphere,diffused} \qquad (2\text{-}20)$$

$$n_{sphere,total} = (1 - \bar{\delta})\frac{n_{source}R^2}{4r_{total}^2} + \bar{\delta}\frac{n_{source}R^2}{4r_{last}^2} \qquad (2\text{-}21)$$

If the following approximation $r_{last} = \frac{r_{total}}{(N+1)}$ is made, r_{last} is then the "mean free path" and N is the reflection depth, then the Equation (2-21) becomes:

$$n_{sphere,total} = \frac{n_{source}R^2}{4r_{total}^2}(1 + 2N\bar{\delta} + N^2\bar{\delta}) \qquad (2\text{-}22)$$

Defining the ratio $K = \frac{n_{sphere,total}}{n_{source}}$ an equation for the radius R can be defined as:

$$R = \sqrt{\frac{4r_{total}^2 . K}{1 + 2N\bar{\delta} + N^2\bar{\delta}}} \qquad (2\text{-}23)$$

The radius R of the detection disc depends on r_{total} the distance covered by the particle from the source to the sphere, K the ratio of particles that one wants to collect, $\bar{\delta}$ the mean diffusion coefficient and N the reflection depth. This means that it gives a formula for a growing sphere over the propagation depth.

This formula has been implemented in the particle tracing algorithm to define the adaptive spherical collector radius.

The problem with this radius formulation is that it will be limited for a receiver which is close to an object, or a wall. Indeed if the collecting sphere contains an object then it has to be taken into account and the sphere cannot expand outside the room because there is no particle outside but it has to be able to grow without

exceeding the room limits, c.f. Figure 2-9. The next step of the particle tracing model is to introduce a truncation of the sphere exceeding the limits of the room.

Even if this radius formulation has some limitations due to approximations, it gives a way to make the sphere grow.

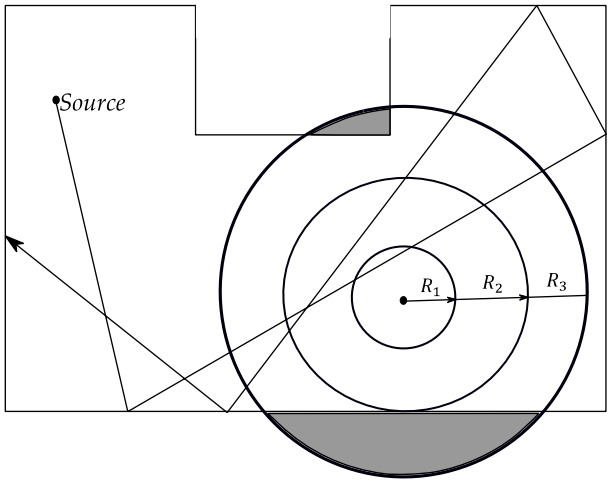

Figure 2-9: Example of a growing sphere which exceeds the limits of the room

Where R_1, R_2, R_3 are respectively the radius after 1, 2, 3 reflections.

2.2.5 Truncation of the collecting sphere

As it has been said in § 2.2.4, the collecting sphere should be able to grow without exceeding the room limits and without encompassing any object. Indeed if the collecting sphere exceeds the limits of the room, as one can see in Figure 2-9, two scenarios could happen: the first one is that the exceeding part of the collecting sphere will never collect any particle and the global energy will be underestimated because of this exceeding volume; the second scenario is that the exceeding part of the collecting sphere could collect inexistent particles behind the room's limits. For these reasons it has been decided to implement, in the particle tracing algorithm, a truncation of the sphere which exceeds the limits of the room.

Geometric or probabilistic approaches would be too complicated to define the volume of the truncated collecting sphere (or more specifically the surface of the truncated detection disc). So it has been decided to use a ray tracing method to estimate this surface.

At the position of the receiver a ray tracing is done to estimate the surface of the truncated disc:

- Rays are emitted in a hemisphere sampled with inclinations angles Θ and azimuth angles ϕ to define all the detection disc orientations. The disc is said to be "oriented" when it is perpendicular to incident directions of particles.

- For each orientation of the detection disc N_Ψ rays are emitted from the center of the disc in N_Ψ directions to calculate the distance to the closest object or wall. A square value $d^2(\Theta, \Phi, \Psi)$ (or infinite in case of open range) of this distance is stocked.

In Figure 2-10 one can observe a detection disc projection (i.e. fixed values of Θ and ϕ) and the N_Ψ rays emitted to define the truncated disc. The surface of the truncated disc is then approximated using the minimum value between the $d^2(\Theta, \Phi, \Psi)$ value calculated by this ray tracing calculation and the R^2 value calculated using Equation (2-23). Finally it gives a 3D diagram of the truncated collecting sphere.

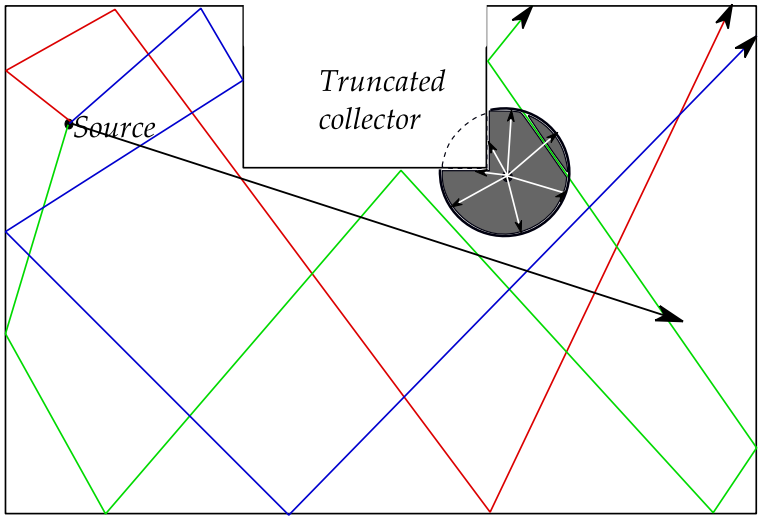

Figure 2-10: Example of the calculation of the truncated disc surface

2.2.6 Surface storage

A problem with the spherical collector described in the previous paragraphs is that it is not sure to collect some particles paths which last reflection is diffused. To describe these paths a grammar representation of the propagation path is used [18], [22]. This grammar is also used to describe any possible paths (direct paths, specular paths, diffused paths …).

Direct path	**E-R**
Ray tracing **Beam tracing** **Image sources**	**E-S*-R**
Particle tracing	**E-[S|D]*-R**

- E : Emission
- R : Reception
- S : Specular reflection
- D : Diffuse reflection
- * : zero reflection or more
- | : one element or the other

Table 2-1 : description of the grammar representation

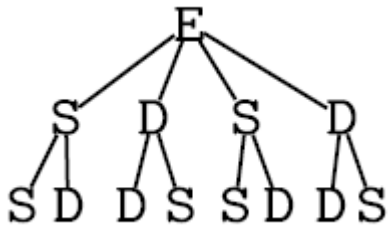

Figure 2-11: Tree representation of the propagation paths

A path whose last reflection is diffused will be written E-[S|D]*-D-R. It is not sure that these paths will be collected by the collecting sphere since after a diffuse reflection a particle is reflected in a random direction and it is possible that it misses the collector. Therefore the spherical collector will be used for E-[S|D]*-S-R type of paths (a path whose last reflection is specular) and surface collectors placed on the room walls will be used for E-[S|D]*-D-R types of paths.

The surfaces of the room are meshed and each face of the mesh acts as a surface collector which records the energy of the paths which end up with a diffuse reflection. The energy is recorded as an impulse response at the centre of the area which has held the diffuse reflection and not at the real impact of the particle; because of this the surfaces need to be finely meshed. If one does not mesh the room surfaces then all the diffuse reflection will be located at the centre of these surfaces and there will be some important delays in the echograms. The meshing discretisation needs to be proportional to the temporal discretisation of the echogram.

2.3 Description of the different steps to model a room acoustic impulse response within ICARE

This part describes the different calculation steps in ICARE for modeling an impulse response of a room. The purpose of this part is to understand what the input data are and how these data are processed at each step of the different calculations.

2.3.1 Input data

An .nff file is used to define the room's geometry: sources and receivers coordinates, definition of the room's surfaces listed as group of material, the diffraction edges …

Another file describes the material properties. For each material one needs to define for every frequency bands:

- Absorption coefficient α_i, with $i = 1,2,3, \dots N_f$ the number of frequency bands
- Diffusion coefficient δ_i, with $i = 1,2,3, \dots N_f$

Another file describes the sources power W_i with $i = 1,2,3, \dots N_f$. The same file can be used to describe the sources and receivers directivity.

2.3.2 Beam tracing

The beam tracing principles are described in part 1.2. This part describes the energy carried by a beam along its propagation.

A beam j has an initial energy $e_{ij}^{(0)} = \frac{W_i \Omega_j}{4\pi}$, with Ω_J the opening angle of the beam j. After *N* reflections the beam's energy becomes:

$$e_{ji}^{(N)} = \frac{W_i \Omega_j}{4\pi} \cdot (1 - \alpha_{1i}) \frac{(1 - \delta_{1i})}{1 - \overline{\delta_1}} \cdot (1 - \alpha_{2i}) \frac{(1 - \delta_{2i})}{1 - \overline{\delta_2}} \cdot \dots \cdot (1 - \alpha_{Ni}) \frac{(1 - \delta_{Ni})}{1 - \overline{\delta_N}} \qquad (2\text{-}24)$$

with $\overline{\delta_N} = \frac{1}{N_f} \sum_{i=1}^{N_f} \delta_{Ni}$

The contribution of each beam at the receiver position is expressed with the following Equation (2-25):

$$p_i^2 = \frac{\rho_0 c \cdot e_{ij}^{(N)}}{4\pi} G^2 \cdot \delta[t - \frac{r^{(N)}}{c}] \qquad (2\text{-}25)$$

Where:

$r^{(N)}$ is the distance from the source to the receiver along the ray path after N reflections;

G is the Green's function and can be expressed as $G = \prod_{i=1}^{N} R_i \times \sqrt{\frac{d\Omega}{dS}}$ with R_i the reflection coefficient of the i[th] reflection;

$d\Omega$ is the initial solid angle from the punctual source as one can see on Figure 1-2;

dS is the wave front's surface at the receiver's position defined by the three supporting rays of the beam as described in § 1.2.1.

In Equation (2-25), $\delta[t]$ is the Dirac function and not a diffusion coefficient.

When one takes into account the diffraction phenomena, the Green's function calculation is a lot more complicated and is not detailed here.

The beam tracing is a purely geometric calculation which gives all the specular reflections until a maximum propagation depth N_{spec} and the diffracted paths (limited to a N_{diffr} number of diffraction per propagation path). As it is explained in paragraph 1.2.2, it's the "acoustic" calculation which takes into account the material properties, the frequency dependence, and the directivity of the sources and/or receivers …

2.3.3 Particle tracing algorithm

This paragraph describes the different steps of the particle's energy calculation along the particle's propagation in the room. One has to notice that this calculation is done one time for all the frequency bands. The values e_i which correspond to the energy of particles for the ith frequency band are calculated during the same calculation for all the frequency bands and are all stocked in matrix.

- The source emits n_{source} so the initial energy of a particle is

$$e_i^{(0)} = \frac{W_i}{n_{source}} \qquad (2\text{-}26)$$

At each reflection N a random number z is drawn, $z \in [0; 1]$:

- if $z < \overline{\delta_N}$: diffuse reflection, i.e. random drawing with a projected solid angle
- if $z > \overline{\delta_N}$: specular reflection

- The energy of a diffusively reflected particle after the reflection is:

$$e_i^{(N+1)} = e_i^{(N)}(1 - \alpha_i)\frac{\delta_{Ni}}{\overline{\delta_N}} \qquad (2\text{-}27)$$

- The energy of a specularly reflected particle after the reflection is:

$$e_i^{(N+1)} = e_i^{(N)}(1 - \alpha_i)\frac{1 - \delta_{Ni}}{1 - \overline{\delta_N}} \qquad (2\text{-}28)$$

With $\overline{\delta_N} = \frac{1}{N_f}\sum_{i=1}^{N_f}\delta_{Ni}$

With this formula one can notice that during the propagation of a particle, the energy of this particle could be larger than its initial energy. But since a stochastic approach is used (c.f. Monte Carlo's principles [6] [7]) the global energy will be averaged between all the particles and will converge to a lower value than the initial energy.

The choice of $\overline{\delta_N}$, which determines if a reflection is diffuse or specular, is arbitrary and other solutions could have been chosen. However one has to notice that it will not affect the diffuse behaviour of the material since the way of choosing between a specular or a diffuse reflection is compensated by the weight allocated to the different particles [9]. Indeed the energy of a diffused particle is weighted by $\frac{\delta_{Ni}}{\overline{\delta_N}}$ and the energy of a specular particle is weighted by $\frac{1-\delta_{Ni}}{1-\overline{\delta_N}}$. The mean value of each e_i will tend to mathematically correct results [6], [7], [9].

- The energy stored by the spherical collector which has received n_{sphere} particles is:

$$p_{sphere}^2 = \rho_0 c \sum_{i=1}^{n_{sphere}} \frac{4 \cdot e_i}{\pi R^2} \qquad (2\text{-}29)$$

This leads to the following Equation (2-30) for the expectation of the pressure received by the collecting sphere:

$$\langle p^2 \rangle = \langle n_{sphere} \rangle \frac{4 \cdot \langle e_i \rangle}{\pi R^2} \qquad (2\text{-}30)$$

Where $\langle ... \rangle$ denotes the mean of a function.

- For the truncated collector the received energy is not the same, indeed the surface of the disc is no longer πR^2 but it depends on the geometry of the room as explained in § 2.2.5.

The disc is still growing according to Equation (2-23) described in § 2.2.4, then one needs to take the minimum value of the values $R^2(t)$ and $d^2(t, \Theta, \Phi, \Psi)$ (c.f. § 2.2.5) to calculate the truncated disc surface. This leads to the following Equation (2-31) of the truncated surface:

$$S(t, \Theta, \Phi, \Psi) = \frac{2\pi}{N_\Psi} \sum_{i=1}^{N\Psi} \frac{\min[d_i^2(t, \Theta, \Phi, \Psi), R^2(t)]}{2} \qquad (2\text{-}31)$$

Moreover the Equation (2-30) becomes:

$$\langle p^2 \rangle = \langle n_{sphere} \rangle \frac{4 \cdot \langle e_i \rangle}{S(t, \Theta, \Phi, \Psi)} \qquad (2\text{-}32)$$

- For every particle going through the sphere if:

- its path is 100% specular with $N < N_{spec}$ **and/or**
- the last reflection is a diffused reflection,

→ Then the particle is ignored by the collecting sphere. Indeed the beam tracing and the surface storage already take these cases into account. Otherwise the particle's contribution is stored at a time $t = t_0 + \sqrt{(t_D - t_0)^2 + c^2\Delta^2}$ which is the time that the particle would take to come from an image source position to the center of the detection disc, see Figure 2-7.

2.3.4 Surface storage

As explained in § 2.2.6, if the room is meshed each mesh can act as a surface collector which records the energy e_i of the particle arriving on this mesh as a "temporary" echogram at the centre of the mesh Each of these temporary echograms will be added to the global echogram but delayed by the time needed for the sound to travel from the centre of the mesh to the receiver position.

The sound pressure expectation $\langle p^2_{mesh} \rangle$ received by one mesh and transferred to the receiver position will contribute to the global echogram as expressed in Equation (2-33):

$$\langle p^2_{mesh} \rangle = \frac{4}{r^2_{mesh}} \langle e_i \rangle \, \delta(1-\alpha) \cos\theta \qquad (2\text{-}33)$$

Wherein r_{mesh} is the distance from the centre of the mesh to the receptor's position and θ is the angle defined in § 2.2.3.

The different calculations through the beam tracing and the particle tracing with a sphere collector and a surface collector should collect accurately every kind of paths.

Indeed **from 0 to N_{spec}**, which corresponds to the early part of the impulse response, the beam tracing models the specular reflections of the impulse response (E-S*-R paths). In this part of the echogram the particle tracing models the E-[S-D]*-D-[S-D]*-R paths, i.e. the paths which contain at least one diffuse reflection. The diffuse reflections modeled by the particle tracing are added with the specular contributions calculated by the beam tracing.

For $N > N_{spec}$ the particle tracing calculations models every kind of paths and gives the late part of the echogram, Figure 2-12.

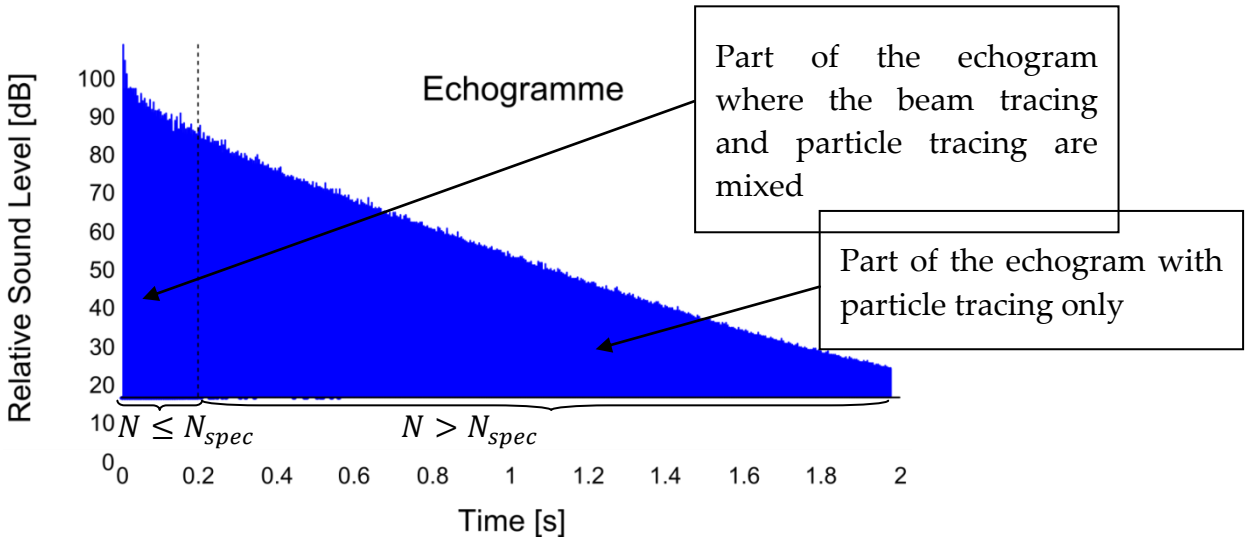

Figure 2-12: Example of an echogram with ICARE

2.4 Validation of the diffuse reflection model

The following paragraphs of this chapter present the successive steps which have led to the final particle tracing algorithm in order to test the influence of different parameters such as the size of the receiver, the initial number of particles emitted by the source, the number of particles received by the receptor, the number of calculation steps, the truncation of the collecting sphere, etc…

2.4.1 First version of the algorithm: tests on simple plates

The first version of the algorithm was a simple particle tracing calculation with four input parameters: a constant value for the collecting sphere radius, the number of particle emitted by the source, the number of steps in the calculation and the length of each step in the calculation. There was also the possibility to use the surface storage.

For this version the tests have been conducted on finite and infinite plates as one can observe on Figure 2-13 and Figure 2-14. For each of these plates a meshed model has been created in order to test the surface storage option. The finite and infinite dimensions have been investigated in order to check that the algorithm creates impulse responses which are coherent with the dimensions of the plate.

On these plates a 50% absorption coefficient and 50% diffusion coefficient have been implemented for all the frequency bands.

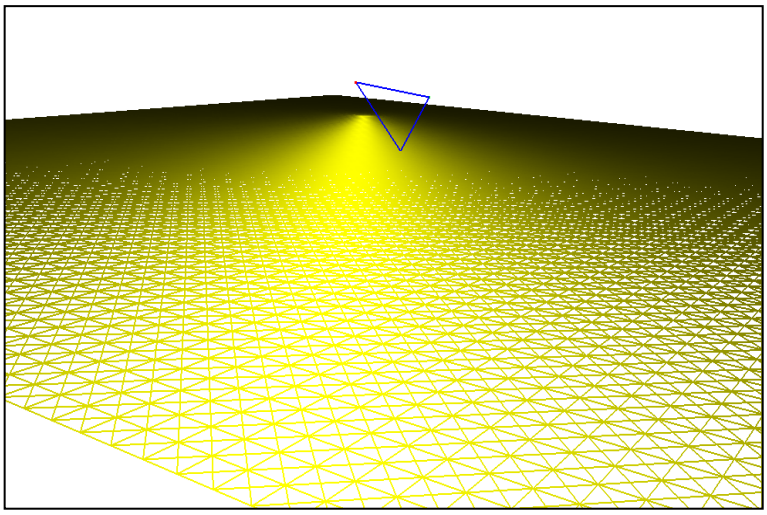

Figure 2-13: Model of a finite plate with mesh

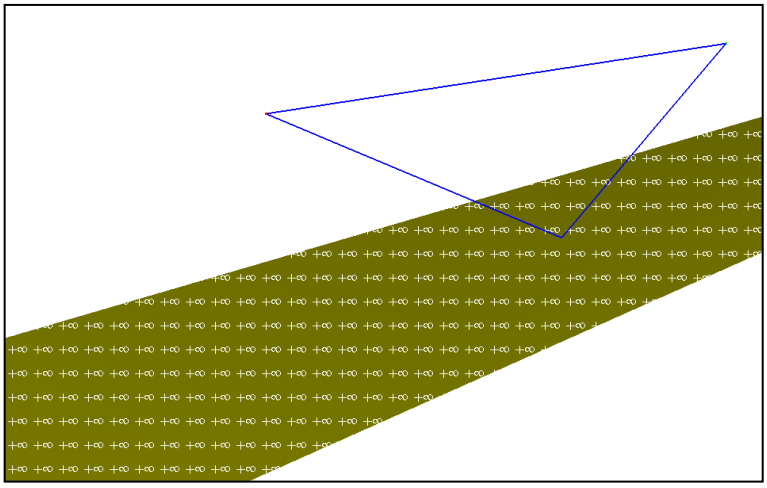

Figure 2-14: Model of an infinite plate without mesh

- **Influence of the detection disc radius**

The Figure 2-15 presents echograms obtained with different values (in meter) for the radius of the detection disc. On this figure one can observe that the smaller the radius is the more particles will be missed. It seems also that the initial energy emitted by the source is well split among the detected reflections. Indeed with a radius of 0.8 m the reflection peaks are lower because a lot more reflections are detected.

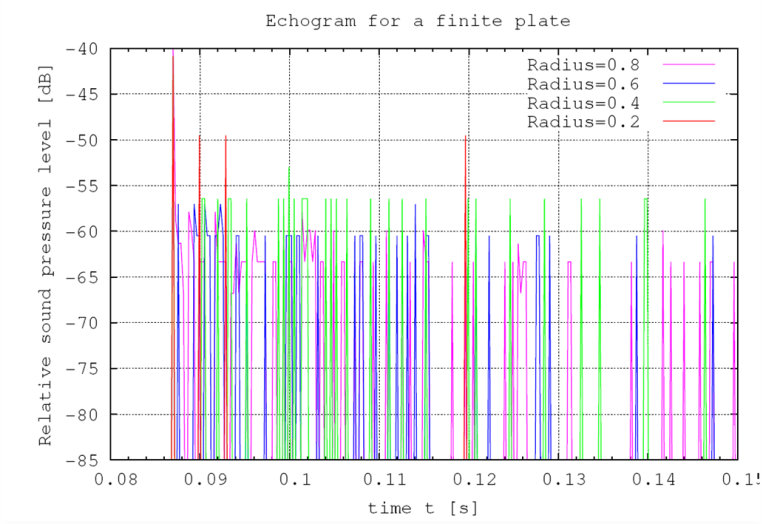

Figure 2-15: Influence of the detection disc radius (in m) on the echogram of a finite table.

- **Influence of the number of particles emitted**

The number of particles emitted by the source has also a large influence on echograms, see Figure 2-16. Indeed it is obvious that the more particles are emitted from the source, the more particles will be detected by the collector. This is called the "law of large numbers" in probability theory. On Figure 2-16 the echogram obtained with ten millions of particles is much richer than the other ones.

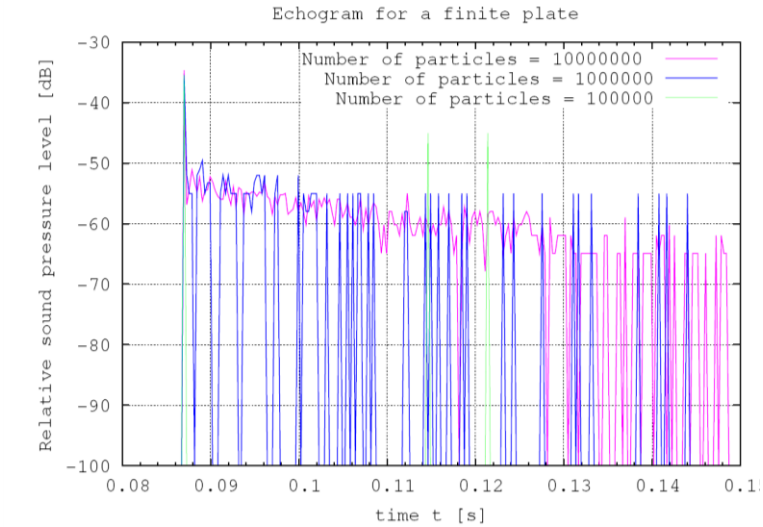

Figure 2-16: Influence of the incident number of particles on the echogram of a finite table

- **Influence of the surface storage**

On Figure 2-17 one can see the comparison between an echogram obtained with only a spherical collector and an echogram obtained with both spherical collector and surface storage (c.f. Paragraph 2.2.6). The blue curve (with the surface

storage) shows what it could have been expected for a finite diffusing and absorbing plate echogram, i.e. a smooth echogram decaying in time until a maximum time value, whereas the pink curve is noisy and incomplete.

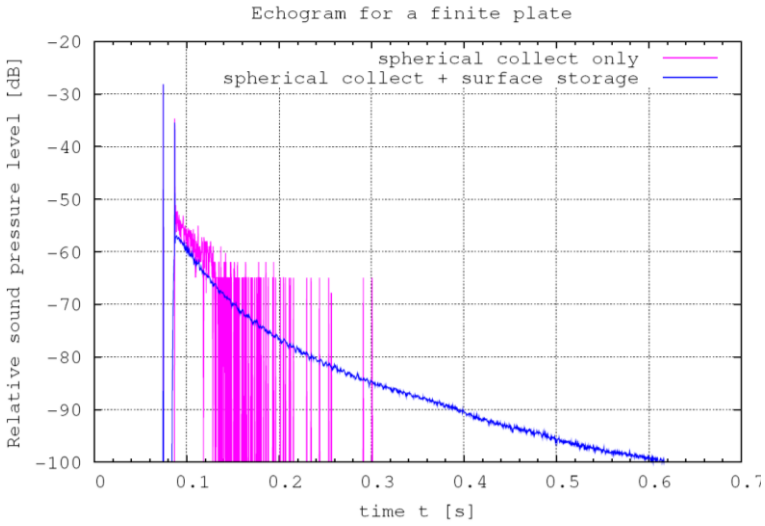

Figure 2-17: Influence of the surface storage on the echogram of a finite plate with mesh

This Figure 2-17 proves the efficiency of the surface storage to obtain a smooth echogram. It also shows that a constant spherical collector is not adapted to detect enough particles and to obtain an accurate echogram unless to emit a very large number of particles from the source.

2.4.2 Version of the algorithm with a growing collector

The surface storage is quite time consuming for the calculations (and is limited to improve diffusion-ended paths) and a constant radius for the collecting sphere requires emitting a very large number of particles to obtain a correct echogram. For these reasons a growing collecting sphere has been implemented using Equation (2-23) to improve the detection of the particles and the precision of the echograms.

For this version of the algorithm the input parameters were the number of particles, the number of calculation steps, the length of a calculation step and the ratio K between the number of particles detected by the detection disc and the number of particles emitted by the source. Moreover this version of the algorithm used a beam tracing calculations for the early specular reflections of the echogram and mixed these calculations with the particle tracing calculations for the diffuse contributions, which gives the late part of the echogram. This paragraph will focus specifically on the part of the echogram modelled by the particle tracing only.

- **Test on a simple four walls room**

To check the right functioning of the algorithm, it has been tested on a simple four walls room with unparalleled walls, to avoid flutter echo. The volume of this room is $V = 460\ m^3$, its total surface is $S = 379\ m^2$ and $\alpha = 0.1$ as the absorption coefficient on every wall. The following reverberation time value could be expected:

$$RT = 0.161\frac{V}{\alpha S} = 1.95\ s$$

Our simulation with ICARE gives a RT value of 1.90s at 1000 Hz.

For $\alpha = 0.2$ the algorithm gives a calculated RT value of 0.9 s compared to a theoretical value of 0.97 s.

This test shows that the algorithm works reasonably well or at least that the algorithm heads toward a good direction.

- **Tests on Round Robin III models**

The Round Robin test is used by developers and users of computer simulation software to assess their results with the measured results on the same object [23]. The considered Round Robin test is the third one to be done on Room Acoustical Computer Simulation. In this third Round Robin test the music recording studio of the Physikalisch-Technische Bundesanstalt Braunschweig, Figure 2-18, served as simulation object. It uses three model phases of this room with increasing geometrical details, see Figure 2-19.

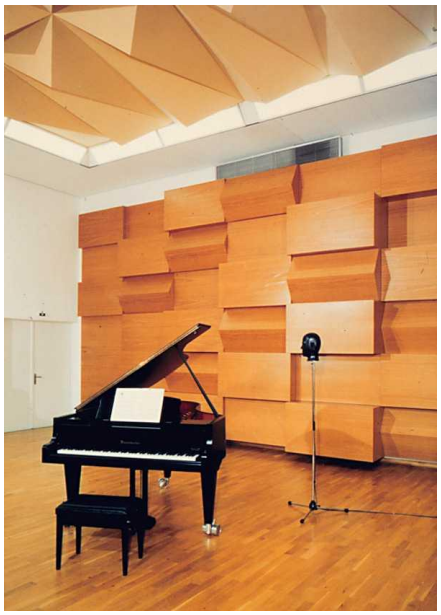

Figure 2-18: Music recording studio of the Physikalisch-Technische Bundesanstalt Braunschweig, c.f. [23]

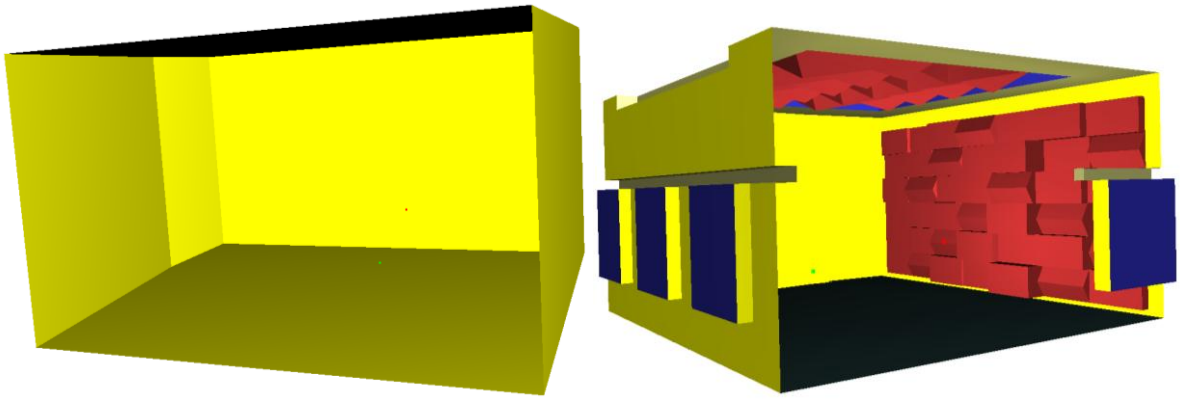

Figure 2-19: Round Robin III models in ICARE – phase 1 (left) and phase 3 (right), c.f. [23]

The following figures, Figure 2-20 to Figure 2-23, introduce tests conducted on Round Robin III (RR3) phase 1 model which is the simplest model of the third Robin with only five walls, a floor and a ceiling. An absorption coefficient of 0.1 and a diffusion coefficient of 0.1 are applied on every wall of the room.

Figure 2-20 and Figure 2-21 show the effect of a growing radius of the detection disc with the reflection depth. As shown in § 2.2.4 the radius depends on the ratio *K* between the number of particles detected by the detection disc and the number of particles emitted by the source.

On Figure 2-20 the influence of the ratio value is significant. A 60% ratio value gives a growing detection disc which detects more particles and gives an echogram richer than the ones obtained with the 20 to 50% values.

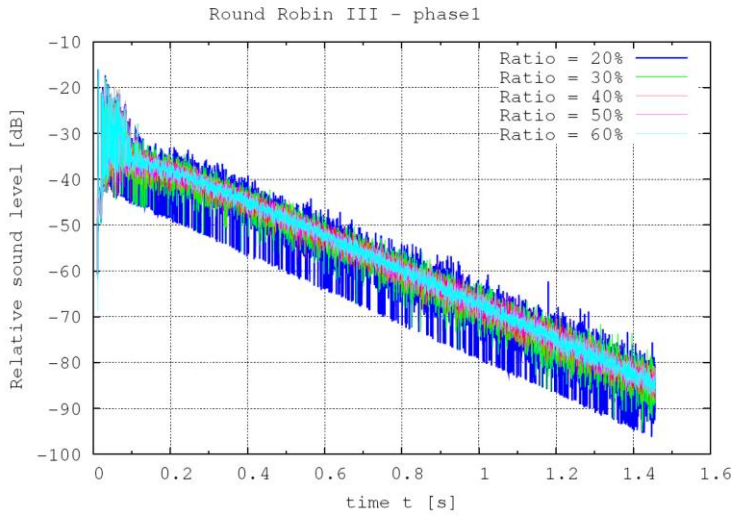

Figure 2-20: Variations of the RR3-phase1 echograms with the ratio K between 20% and 60%

However on Figure 2-21 it can be observed that a ratio value from 70% to 100% does not affect the echogram at all. This is due to the fact that in this version of

the algorithm the radius of the detection disc can grow but cannot exceed the limits of the room. For a bigger ratio than 60% the detection disc radius has already reached these limits and cannot grow further.

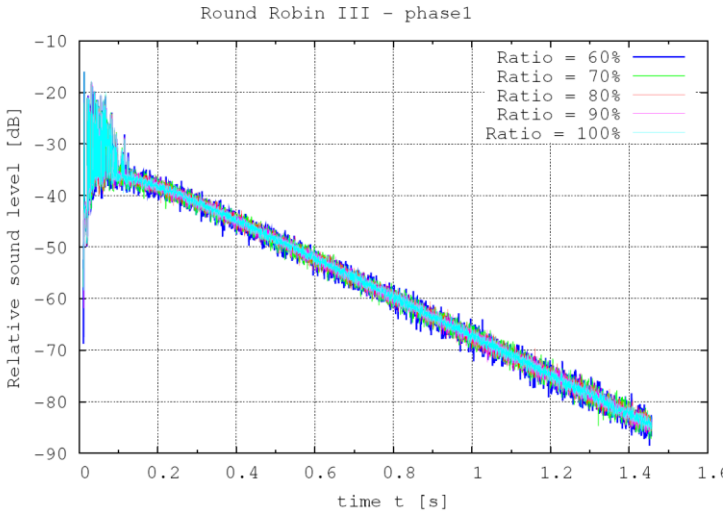

Figure 2-21 : Variations of the RR3-phase1 echograms with the ratio K between 60% and 100%

Figure 2-22 illustrates two echograms of the RR3 phase 1 obtained with the same ratio $K = 60\%$ but with different number of emitted particles. In blue the echogram obtained with the source emitting one hundred thousand particles and in green the echogram obtained with one million particles. The results with one million particles is still smoother and with less variations but the one with one hundred particles seems quite acceptable since the curve is scattered around the same value than the green curve.

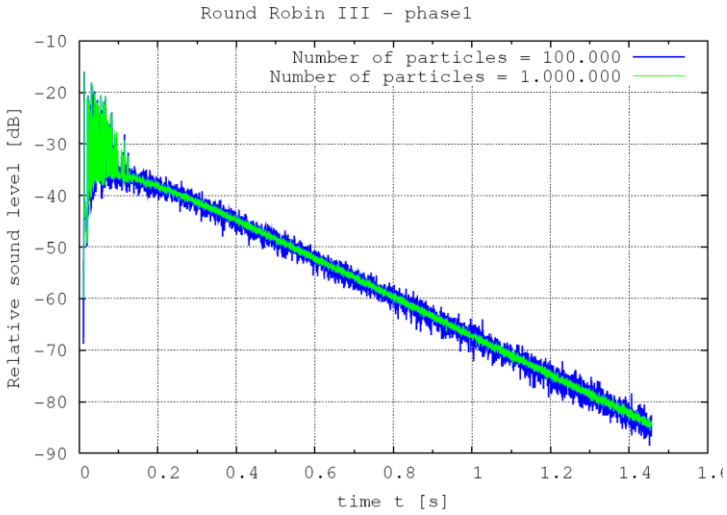

Figure 2-22: Influence of the incident number of particles on the echogram of the RR3 phase 1 echogram

With the particle tracing using only a detection disc with one million particles one can obtain the same result than with the particle tracing using both the detection

disc and the surface storage (which implies to have a meshed geometry) with one hundred thousand particles, see Figure 2-23. Comparing with the results of Figure 2-17 it seems that a growing sphere improves the detection of particles.

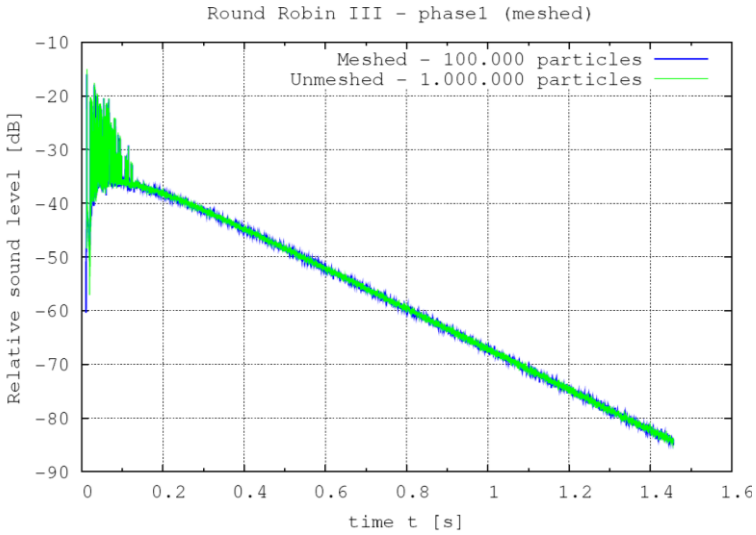

Figure 2-23: Influence of the surface storage on the echogram of the RR3 phase1

2.4.3 Version of the algorithm with a growing and truncated collector

In this version of the algorithm the truncation of the collecting sphere has been implemented. The aim of the following paragraphs is not to prove that the truncation of the sphere will improve the results but it is more to try to show that results obtained using the truncated collector are the same or close than results obtained with a limited collector (i.e. constant or growing but limited by the geometry). Therefore with a truncated collector fewer particles should be needed than with a limited collector to get the same results since the truncated collector continues to grow during the propagation time. The reduction of emitted particles will lead to a decrease of the calculation times. If one does not choose to reduce the number of particles emitted then the calculation times will not be reduced but the precision should be increase.

Another purpose for developing this truncated collector is that a receiver which is really close to a wall will be able to grow if the part of the collector exceeding the limits of the room is truncated. Furthermore, if the growing and truncated collector works independently of the receiver positions then it will simplify the user choices concerning the size of the collectors, the same input parameters will be applied for every receiver even if it is very close to a wall.

The input parameters for this version of the algorithm are still the number of particles, the number of calculation steps, the length of a calculation step, but the ratio K is defined using a definition for the initial size of the growing collector.

Indeed the initial size of the radius can be expressed using the formula of a collecting sphere in a free field, see Eq.(2-34). This equation is derived from Eq.(2-23).

$$R^2_{free\ field} = 4LK \qquad (2\text{-}34)$$

Wherein L is the mean free path, i.e. the average distance covered by particles between two reflections.

The sphere starts growing from this initial size $R^2_{free\ field}$ and then Equation (2-23) is used. Therefore the user will indirectly define the ratio K by choosing a value for the initial size of the growing collector.

To test this new version of the particle tracing, and to be sure that the truncation of the collector does not distort the results, calculations on simple models have been made using a pure particle tracing calculation. These calculations have been compared with a reference calculation using the beam tracing method. Indeed the beam tracing calculation is a determinist approach which gives exact paths between a source and a receiver using a source-image method. Because the beam tracing calculation only models pure specular reflections the particle tracing algorithm has also been used to model only purely specular reflections to be able to compare both approaches. Even if the particle tracing was implemented to model diffusion, no diffusion has been introduced in the following tests to verify that the modified particle tracing algorithm, with the truncation of the collector, modelled the propagation path correctly.

- **Tests on a simple box model**

First of all the particle tracing calculation has been tested on a small box ($V = 3.5\ m^3$), see Figure 2-24, because it was possible to compare it with a beam tracing calculation up to a very high reflection order since it is a simple geometry.

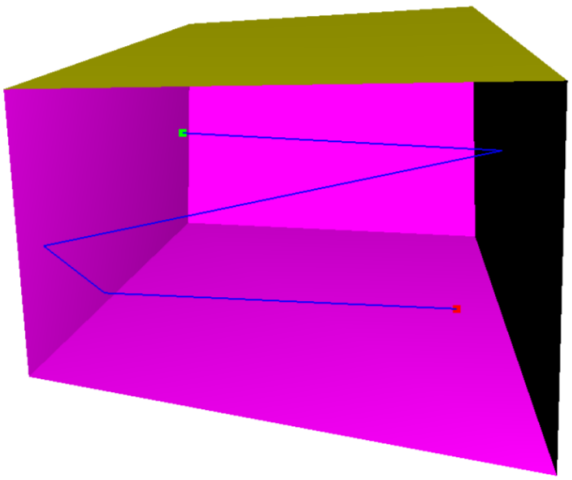

Figure 2-24: Example of a propagation path in the shoe box model

Figure 2-25 compares the echograms for purely specular reflections in the box with the beam tracing approach (blue curve) and the particle tracing approach (red curve). On those figures the beam tracing calculation is the same for each graph and is done up to a $N = 32$ reflection order, however the particle tracing which have led to those echograms differ in the type of collector used:

- Upper left side echogram: collecting sphere with a constant radius $R = 0.05\ m$
- Upper right side echogram: collecting sphere with a constant radius limited by the closest wall from the receiver's position ($R = 0.09\ m$)
- Lower left side echogram: collecting sphere with a growing radius limited by the closest wall from the receiver's position ($R = 0.05\ m \rightarrow 0.09\ m$)
- Lower right side echogram: collecting sphere with a growing radius a truncated collector when exceeding the room's limits

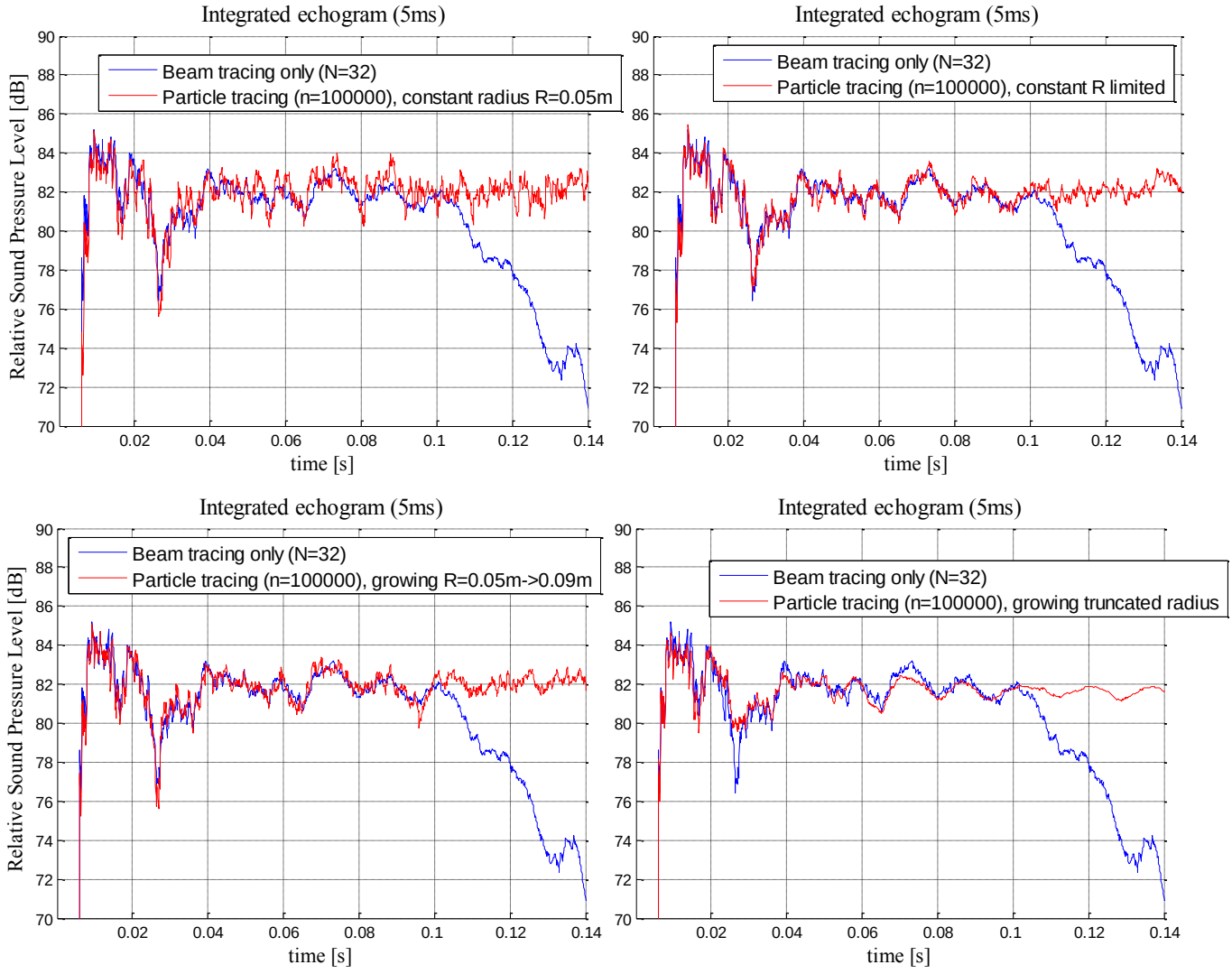

Figure 2-25: Integrated specular echograms for beam tracing (blue) and the particle tracing (red) for a receiver close to a wall

First of all it has to be noticed that the beam tracing which serves as a reference is valid from 0s to 0.1s here. After this value the (blue) curve decays rapidly due to

the fact that higher reflection orders are not modelled here, indeed the maximum reflection order is N=32.

With these integrated echograms it seems that the better calculations, the one which fits better the beam tracing calculation, are obtained with the limited constant radius (upper right side) and the limited growing radius (lower left side). Even if the radius $R = 0.05\,m$ used to obtained the upper left echogram is almost equal to the radius $R = 0.09\,m$ used for the upper right echogram it seems that the energy calculated with the smallest radius is badly approximated.

For the echogram obtained with a growing collector which is truncated when exceeding the limits of the room (lower right echogram) the particle tracing echogram fits quite well the beam tracing one, but not as well as the two others. However those calculations have been made for the worst case scenario, i.e. when the receiver is really close to a wall (here the receiver is at 9 cm distance from a wall).

The same calculations have been made for a receiver which is at the centre of the box (58 cm), see Figure 2-26.

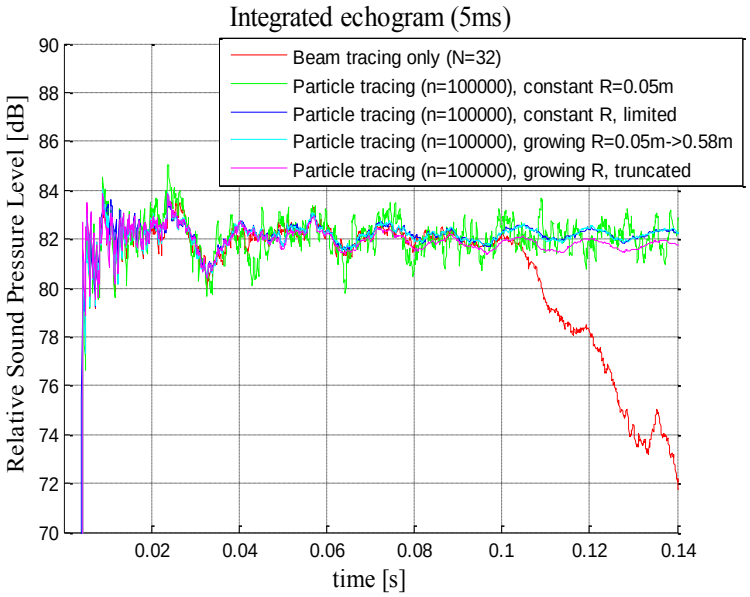

Figure 2-26 : Integrated specular echograms for the beam tracing (red) and the particle tracing (other colours) for a receiver at the centre of the box

On Figure 2-26 it can be pointed out that the integrated echogram obtained with the truncated collector (pink curve) has less energy (the curve is lower) than the others from 0.07s to the end. This observation can also be made for echograms shown in Figure 2-25.

Cumulating the echograms energy over the time is even a better way to realise this difference as one can notice on Figure 2-27.

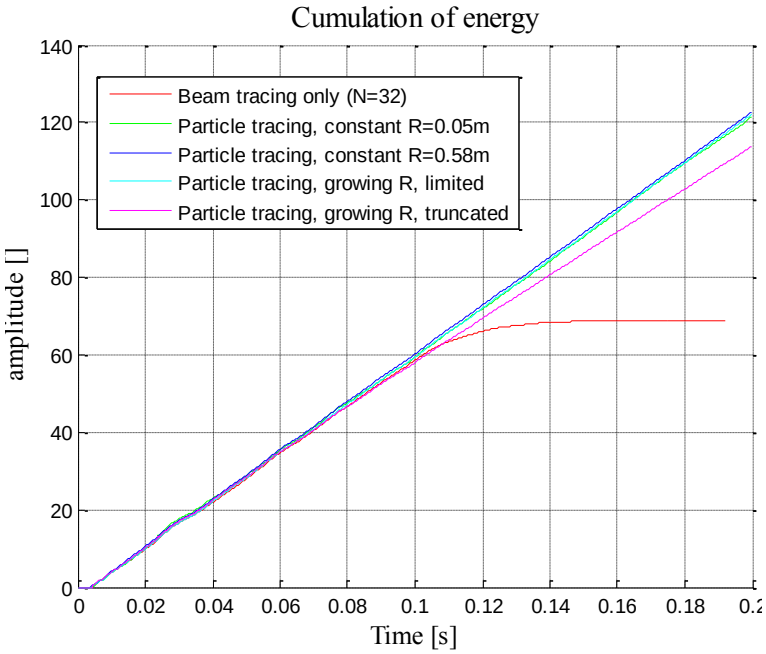

Figure 2-27: Cumulating of energy for the beam tracing calculation (red) and the particle tracing calculations (other colours) for a receiver at the centre of the box

- **Calculations on the Round Robin III**

The same kind of verification tests as for the box have been conducted on the RR3 models, see Figure 2-19, to check that the algorithm worked fine with more complicated and larger geometry. As it has been done for the box model, different calculations of only specular reflections have been realized on the RR3 model:

- A pure specular calculation using beam tracing with N=32 reflection order
- A mixed calculation using beam tracing for the early part of the impulse response, with N=5 reflection order, and particle tracing for the following part of the response, with n=100000 particles
- A mixed calculation using beam tracing for the early part of the impulse response, with N=32 reflection order, and the particle tracing for the following part of the response, with n=100000 particles

Figure 2-28 and Figure 2-29 show the same calculation results but the first one is presented as an echogram (with stems) and the second one as an integrated echogram over 5 ms. It is easier to see with the integrated echogram that the energy at the receiver is almost the same with the different techniques. That means that the specular reflections are well estimated by the particle tracing since it fits well with the beam tracing calculations even for more complex models.

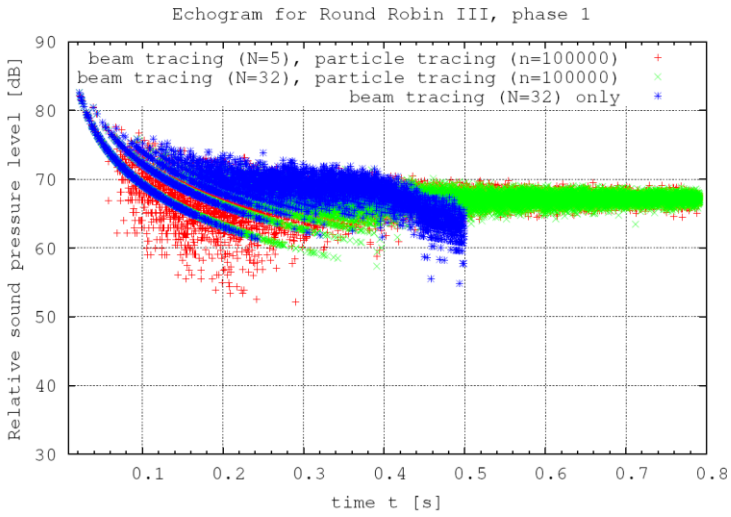

Figure 2-28: Echograms of specular reflections for the Round Robin III-phase1 model

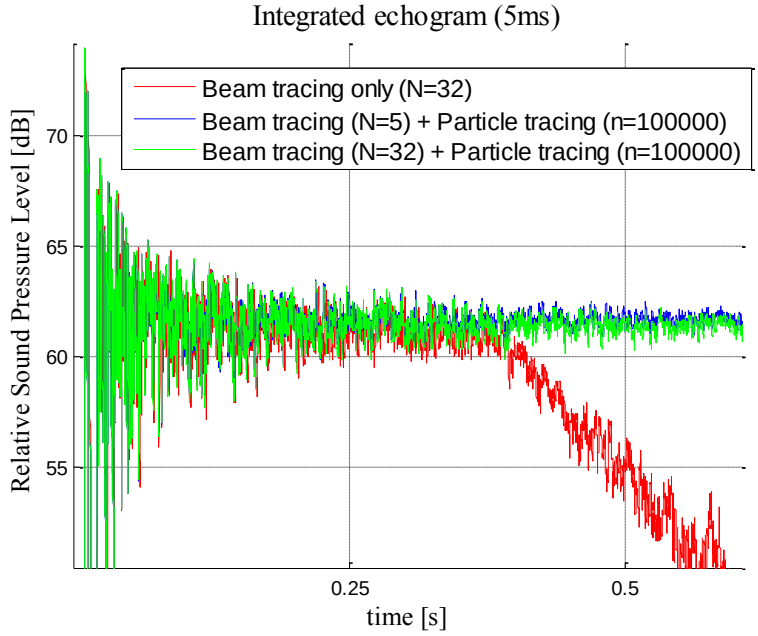

Figure 2-29: Integrated echograms of specular reflections for the Round Robin III-phase1 model

Those figures are interesting in order to see that the particle tracing and especially the collector used in the particle tracing work fine. This means that the collector collects the particle at the right time with the corresponding energy of this particle. But the particle has been implemented to model the diffusion so it would be interesting to see if it fulfils this purpose correctly.

Realistic impulse responses, with absorption and diffusion, have been computed on the RR3 models. The following results have been made using a beam tracing calculation for reflection order up to five and particle tracing for modelling the diffused contributions and the late part of the impulse response.

Figure 2-30 presents the integrated echograms and decay curves for calculations using different types of collector: big constant sphere (red curve), growing sphere limited by the geometry of the room (green curve), growing sphere which is truncated when exceeding the room's limit (blue curve).

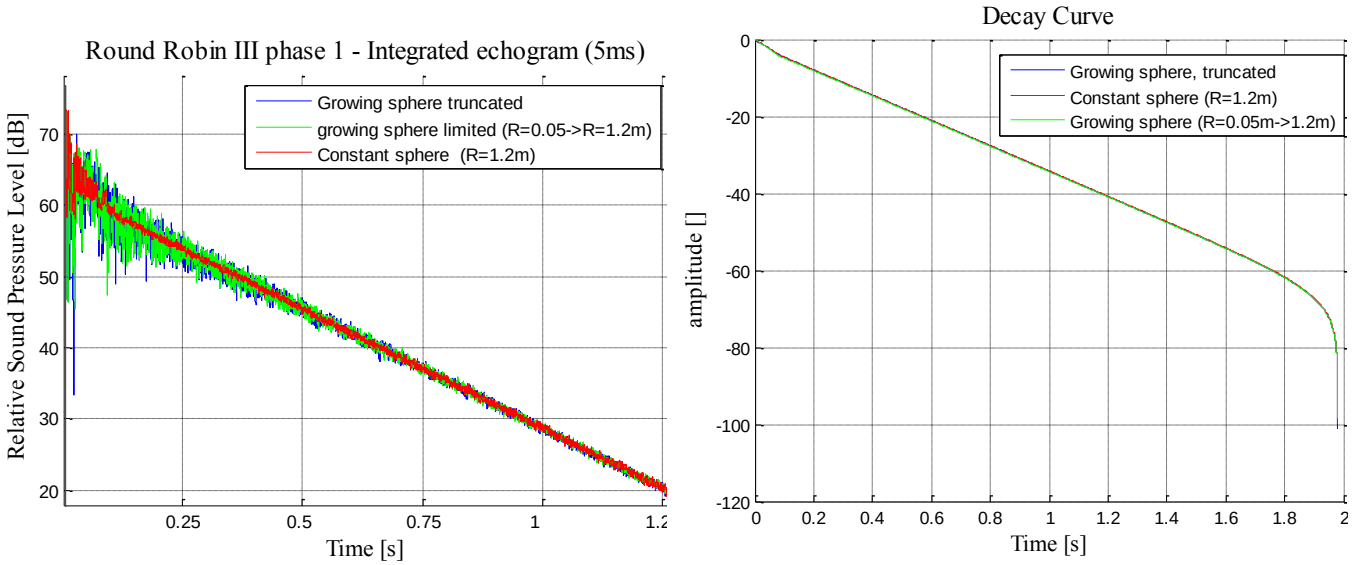

Figure 2-30: Integrated echograms for the Round Robin III-phase1 model

According to Figure 2-30 one could think that a constant sphere with a large enough radius is better than a growing sphere (truncated or not), since it gives less dispersion in the results. But if the early part of the echogram is considered, the influence of taking a big sphere on the first reflection orders can be seen, cf. Figure 2-31. This figure illustrates calculations of specular reflections using beam tracing only (blue curve) and particle tracing only with a growing and truncated collector (red and green curve). The difference between the red and the green curve is that they do not grow from the same initial radius, indeed the red curve has been obtained with an initial radius of 0.05m and the green curve with a 1.2m initial radius.

These results show that having a big collector is not recommended for the first reflections because it gives multiple reflections where there should be only one. However with a collector too small at the beginning some reflections will not be detected (for example the one at 0.021s). Energetically speaking these approaches give the same results, as can be seen on the decay curves on Figure 2-30, but if the calculations shall be used as an input for auralization then the first reflections are of primary importance.

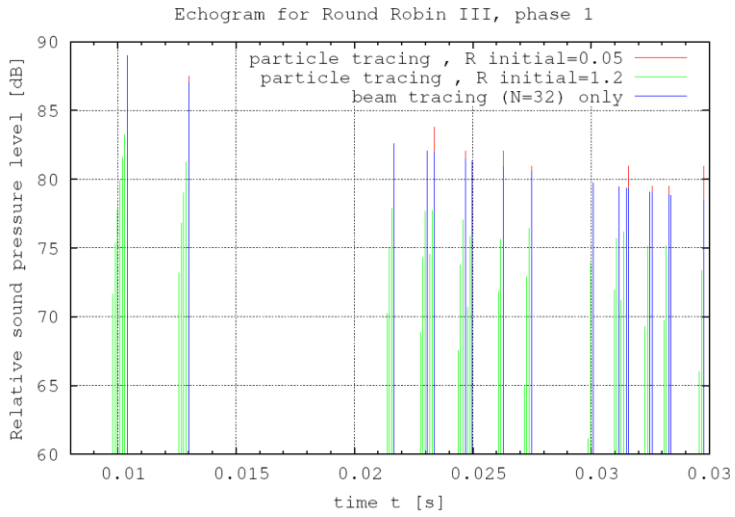

Figure 2-31: Early part of the echograms obtained with the Round Robin model

2.4.4 Comparison with the Round Robin III results

This paragraph introduces some comparisons with the criteria obtained by the Round Robin III study. To compare ICARE results with this study, the mean value of the 21 participants of the study has been used, c.f. [23].

Appendix A: Definition of the criteria presents the definition of the calculated criteria.

These results have been calculated using the algorithm which mixes beam tracing calculations and particle tracing calculation. For the beam tracing a reflection order $N_{spec} = 5$ has been chosen and in the particle tracing the source emitted one hundred thousand particles. Then three different calculation have been made, using three different collectors:

- a constant collecting sphere (green curve “constant radius”)

- a growing collecting sphere limited by the geometry of the room (red curve “limited radius”)

- a growing and truncated sphere (blue curve “truncated radius”)

The results obtained with these different configurations have been compared with the mean value of all the users who participated to this Round Robin test (purple curve “RR3 phase1”). The following figures (from Figure 2-32 to Figure 2-35) represents the comparisons of RT30, EDT, D50 and C80 for the Round Robin III phase 1 model, for the source number 1 and the receiver number 2 (S1R2) for each octave band.

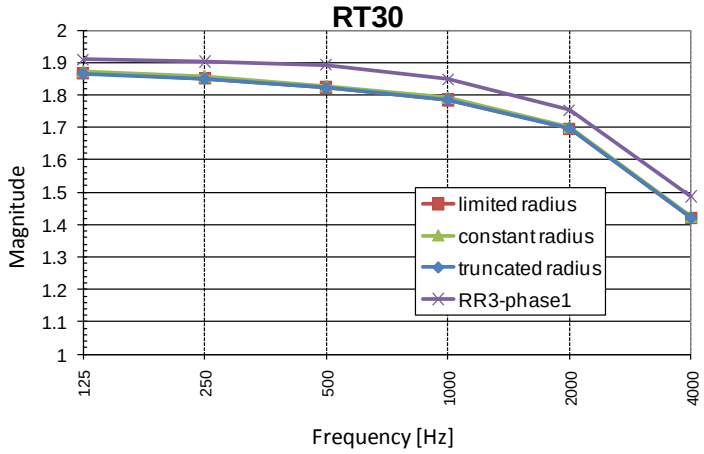

Figure 2-32: Reverberation time for the RR3-phase1 S1R2

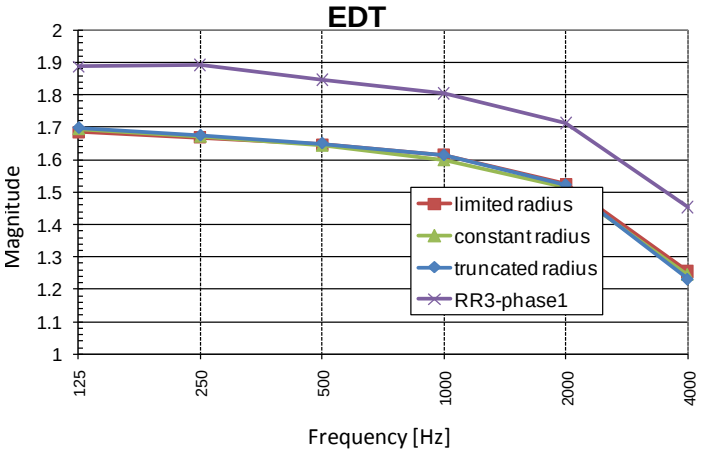

Figure 2-33: Early decay time for the RR3-phase1 S1R2

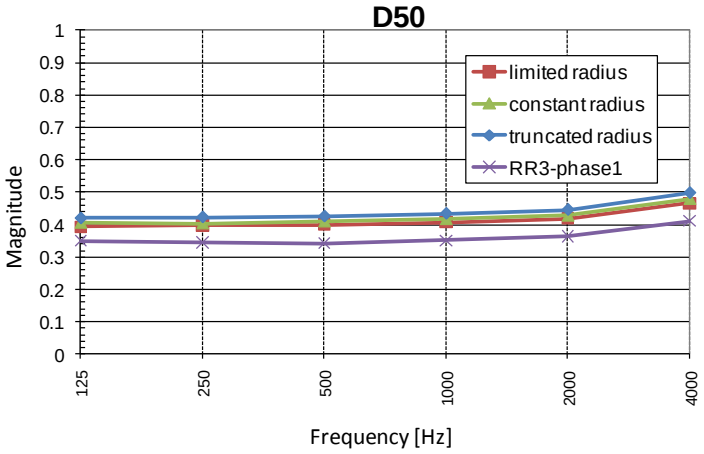

Figure 2-34: Definition for the RR3-phase1 S1R2

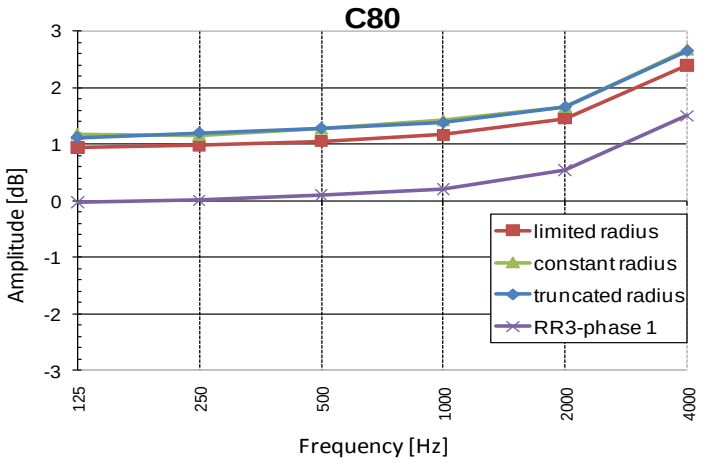

Figure 2-35: Clarity for the RR3-phase1 S1R2

All the criteria results for this configuration are listed in the Appendix B: criteria for RR3-phase1 (S1R2)for each octave bands.

According to these graphs and the table in Appendix B: criteria for RR3-phase1 (S1R2), one can notice that RT30 values are the same depending on the different kind of collector and are very similar with the RR3 mean values. This is also true for the definition D50. However the Early Decay Time (EDT) and the clarity (C80) values obtain with the ICARE's new algorithm is quite different than the RR3 mean values. Furthermore one can observe that C80 values obtained with a growing and truncated collector are higher than the values obtained with the two other collectors.

With those results one can notice that our algorithm gives good reverberation time values but there is still some problem with the calculation of C80 and D50 criteria. Since the criteria calculator that has been used has been validated by a Round Robin test specifically created for criteria calculation [24], it seems that there is a problem with the ICARE's new algorithm or with some input parameters used for this calculation. From this point we did not try to compare other criteria such as the strength G, the lateral fraction LF, the interaural cross correlation IACC but we tried to focus on the reasons in the modelling that could explain differences in criteria such as C80, D50 or EDT.

2.4.5 Transformation of octave band impulse responses to a full band impulse response

As it has been described in part 2.4 the ICARE's results are time dependent and are obtained for each octave band because the particle tracing is a wide band approach. More precisely the absolute values of pressure over time for each octave band are obtained as an output value; see Appendix E for an example of output file. There is no phase information within the particle tracing approach, indeed the particle tracing corresponds to a source which emits impulses that

propagate within the room and are collected by the sphere collector as a sum of impulses over time for each octave band. Energetically speaking, these impulse responses have the information corresponding to their octave band, but if one takes the Fast Fourier Transform (FFT) of these impulse responses to get the Frequency Response Function (FRF), then the frequency information contained in those FRF does not correspond to the octave band considered. This can be explained by the fact that a FFT of a simple impulse in time gives infinite frequency information.

Figure 2-36 shows the FFT of the 1000Hz octave band impulse response which has not been filtered (in red) and the FFT of the same octave band impulse response previously filtered by the corresponding octave band filter.

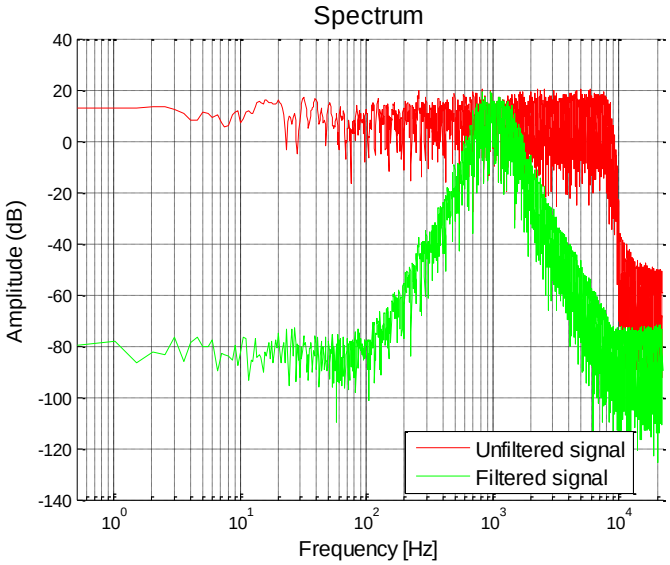

Figure 2-36: FFT of an unfiltered ICARE impulse response (red) and of a filtered one (green)

Therefore for each octave band result one has to:

- reconstitute the phase information
- apply the corresponding octave band filter

Once this has been done for every octave band results, it is possible to sum each octave band result to obtain a real impulse response for the whole frequency band. With this global impulse response one should be able to do auralization convolving this impulse response to an anechoic sound. Figure 2-37 presents the echogram obtain for one octave band as it is obtain after our algorithm calculation (left figure) and the global impulse response which is the sum of the filtrated octave band impulse responses (right figure).

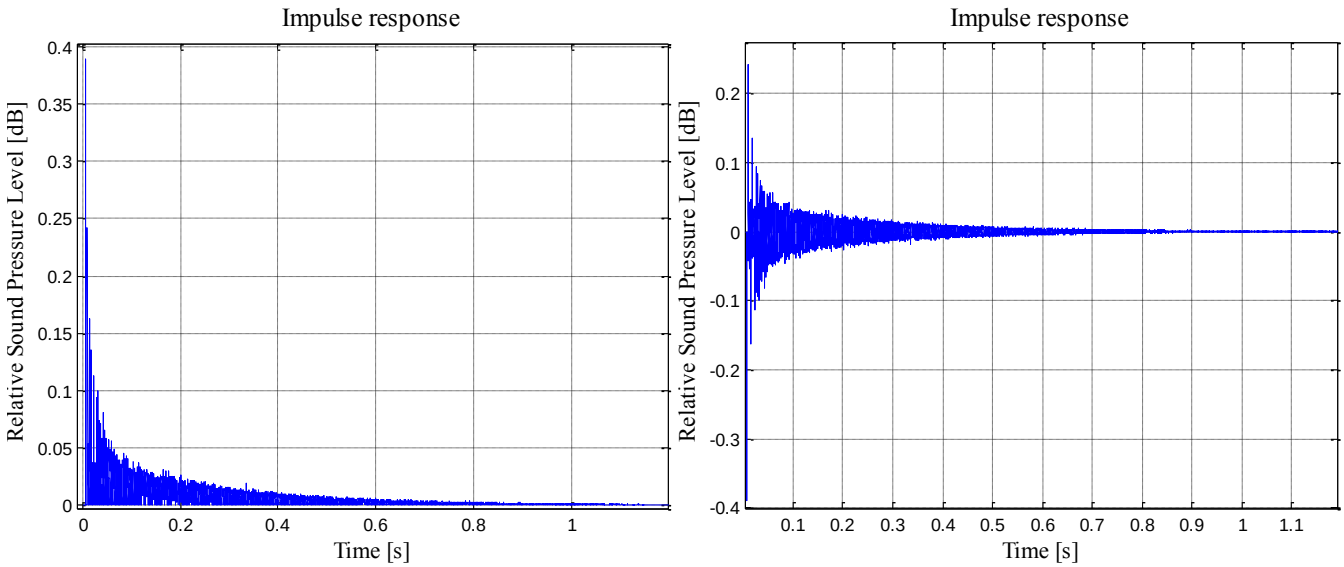

Figure 2-37: ICARE impulse response (left figure) and ICARE impulse response multiplied by random signs (right figure)

The solution applied here to reconstitute the phase information was to multiply random signs with the absolute values of the pressures of octave band impulse responses obtained with ICARE's calculations. With these added random phase one can filter each of the octave band impulse response and sum them to obtain a global impulse response. But the problem with this method is that a "fake" phase information is obtained, i.e. it does not correspond to the real phase that should be obtained in the room.

Therefore the auralization tests made with this global impulse response convolved with an anechoic sound were inconclusive. To get better auralization results one should reconstitute the phase information in a better way.

A solution to reconstitute better phase information for ICARE's impulse responses would be to use the phase information initially calculated in the beam tracing calculation. Indeed the beam tracing calculation used in the algorithm takes the phase into consideration but this phase is suppressed because in the algorithm to mix the beam tracing calculation with the particle tracing calculation energy, i.e. squared pressure values, has been added. When the pressure values from the beam tracing are squared the phase information is lost.

The first part of the impulse response, $N \leq N_{spec}$ (see Figure 2-12) comes from the beam tracing would have the phase information calculated in the beam tracing calculation and the second part of the impulse response, $N \geq N_{spec}$, would have a random phase as described above which should not be a problem since the particle tracing is already based on a stochastic approach.

2.5 Analysis and discussion around the results

As it has been said in the previous part the algorithm seems to model impulse responses which give wrong criteria results when it comes to EDT, C80 or D50 criteria. On the other hand the algorithm seems to work quite well to determinate criteria such as reverberation time (RT30, RT20, and RT10) or TS the centre time.

C80 and D50 criteria are criteria which compare the energy in the different parts of the impulse response, see Appendix A: Definition of the criteria. If the calculation of these criteria is wrongly estimated one could think that the energy is wrongly balanced in the modelled impulse response, that there is too much energy in the early part or not enough for example.

The Figure 2-38 presents accumulation of energy over time for the same calculation than the one describes in § 2.4.4 but using different input parameters in the algorithm. For the different curves on Figure 2-38 different kind of collectors have been used:

- a constant collector with R=0.05m (pink curve)
- a constant collector with R=1.2m (red curve)
- a growing collector limited by the geometry of the room (cyan curve)
- a growing and truncated collector (green curve)

These figures show that the cumulated energy over time is not the same depending on which kind of collector has been used. It seems obvious than the collector with a constant R=0.05m radius is too small to detect enough particles and then it will misses energy in its impulse response. The accumulation of energy obtained with the other three collectors is nearly the same but the truncated collector seems to overestimate the energy as it has been seen in Figure 2-35. This can be due to wrong sampling values when defining the collector's area using a ray tracing method, see § 2.2.5. The collector's area may be underestimated which would lead to an overestimation of the energy received in this truncated collector.

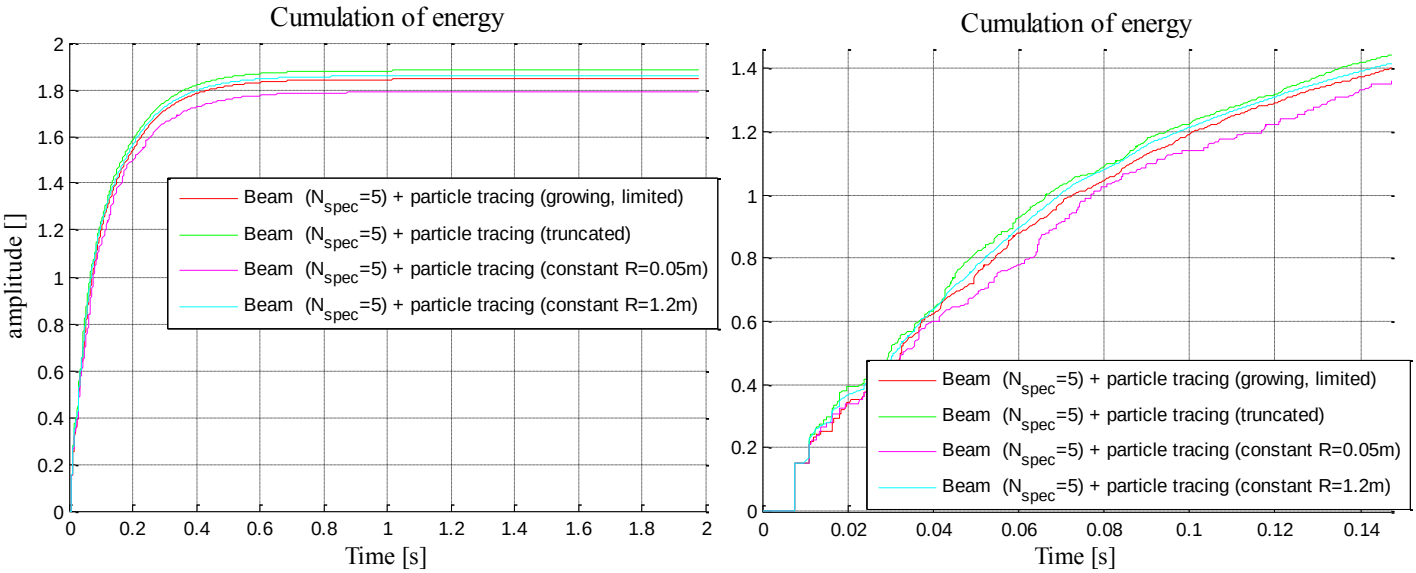

Figure 2-38: Accumulation of energy over the whole time (left) and for the early part of the impulse response (right)

Figure 2-39 shows calculations of the clarity for the RR3 phase1 S1R2 configuration, see § 2.4.4. The different curves have been obtained with different reflection orders N_{spec} which define the beam tracing calculation, see Figure 2-12. The particle tracing parameters are the same for each calculation, i.e. a constant radius R=1.2m for the collector, a constant radius of 0.1m and one million particles emitted by the source.

It seems that the EDT, D50 and C80 calculations converge to the same result as soon as $N_{spec} \geq 15$. See Appendix C: for the results on RT30, EDT, D50 and Ts convergence.

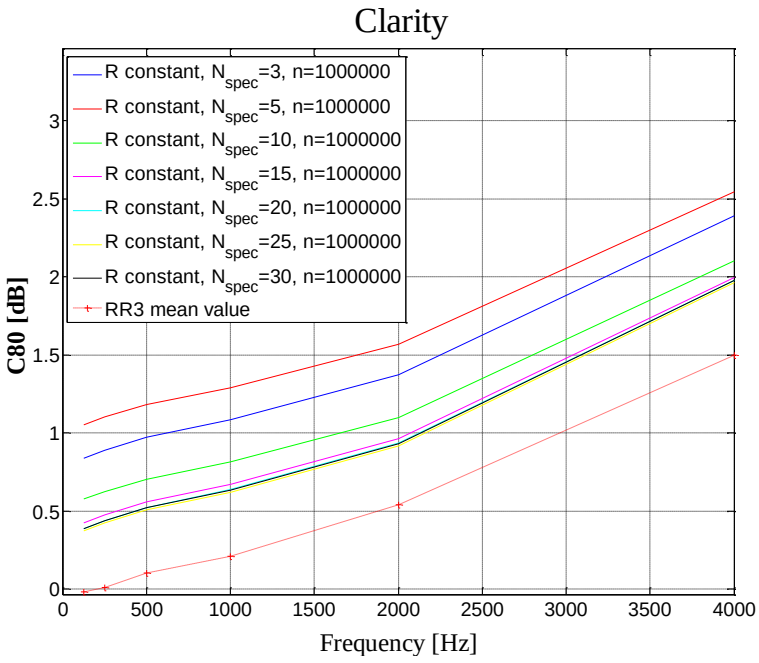

Figure 2-39: Calculation of the C80 for RR3 phase 1 S1R2 with different reflection order

If the C80 values decrease when the specular reflection order of the beam tracing calculation increases, it means that there is more energy in the part of the echogram located after the first 80ms. The Figure 2-40 introduces the energy brought by the beam tracing calculation in the echogram depending on the reflection order. One can observe on this figure that for a reflection order $N_{spec} = 5$ the beam tracing calculation cannot calculate the echogram for the whole first 80ms, there are some missing reflections. Whereas for $N_{spec} = 10$ and $N_{spec} = 15$ the first 80ms are similar which means that the beam tracing calculation covers the early part and that the particle tracing will start modelling specular reflections after these first 80ms.

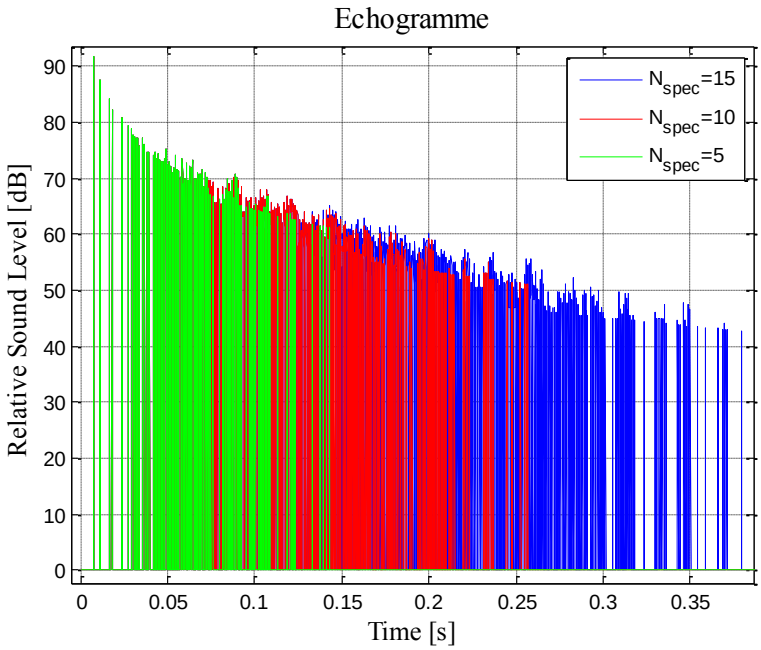

Figure 2-40: Echogram of specular reflections on the RR3 phase1 model using different reflection orders

C80 and D50 criteria are very sensitive criteria and it seems that the reflection order that has been used for the beam tracing calculation will affect these criteria quite much. Since these criteria are so sensitive to the early part of the impulse response it would seem relevant to model the complete early part using a determinist approach like the beam tracing approach.

A reflection order $N_{spec} = 5$, as it has been used for calculations in § 2.4.4, gives wrong values of C80, D50, EDT and Ts. However with a beam tracing calculation done using a reflection order $N_{spec} = 10$ or $N_{spec} = 15$ these criteria are much better and fit quite well with the RR3 mean values. In Appendix D: Criteria and comparison with RR3 phase1 and phase2 results one can see those results and the comparisons between ICARE's calculations and the Round Robin III mean values. For these calculations a reflection order $N_{spec} = 10$ has been used for the beam tracing calculation; and for the particle tracing one million particles have been emitted from the sources and collected by collectors with a constant radius $R =$

0.1 m. The results are an average of all the combinations source/receiver defined in the Round Robin III test, c.f. [23].

These criteria have also been calculated for the RR3 test phase 2 model; see Figure 2-41, with the same calculation parameters as above. These calculated criteria are also presented in Appendix D: Criteria and comparison with RR3 phase1 and phase2 results.

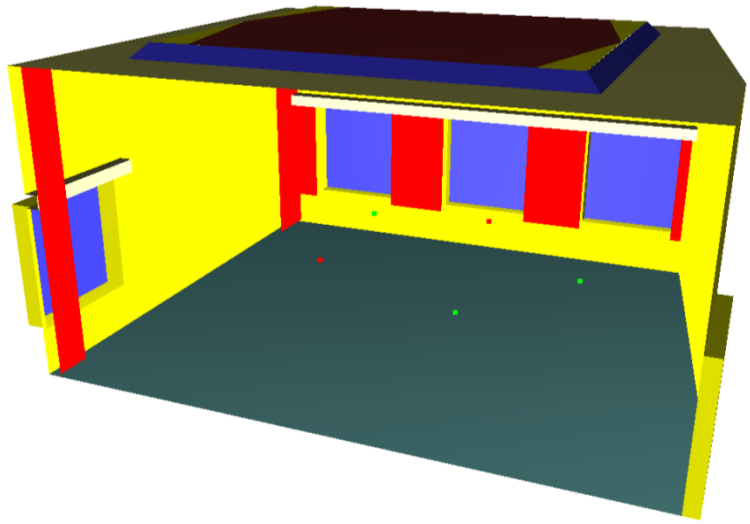

Figure 2-41: Model of the RR3 phase 2

Furthermore the same calculations have been made but with the only difference that a growing and truncated collector has been used for the particle tracing calculation instead of a constant sized collector. For these new calculations the comparisons with the Round Robin test were really satisfying.

Another important aspect that has to be emphasized is that the phase interference phenomena is not modelled within the particle algorithm since only the absolute value of pressure over time has been considered. This phenomenon is taken into account in the beam tracing calculation but is suppressed when it is mixed with the particle tracing calculation. However it seems quite obvious that the phase interference phenomenon is very important for criteria such as clarity or definition and for auralization.

2.6 Conclusion and future work

Finally the criteria obtained with the Round Robin III models and their comparison with all the participant's results are quite satisfying and surely an improvement has been made compared to the criteria which were obtained with the statistic calculation of diffusion and reverberation initially used within ICARE. However the calculations on the Round Robin III phase 3 model have not been made yet and it would be really interesting to compare the ICARE's results

with the results of this phase 3 which model has even more complex details in the geometry.

Furthermore other calculations on bigger and more complex rooms and their comparisons with measurements would validate the correctness of the algorithm for different rooms than the Round Robin models and it would especially validate the right functioning of the growing and truncated collecting sphere for odd room's geometry.

The preliminary auralization tests which have been made have shown the utility to reconstitute the phase information of the signals which is not considered within the particle tracing but in the beam tracing. The only solution tested until now which is to reconstitute the phase information by the multiplication of random signs with the impulse response is not conclusive and another solution has to be found.

3 Inclusion of diffraction in room acoustics simulation

3.1 Introduction

Actually few room acoustics software on the market take into account the diffraction phenomena which happen when the sound wave meets an edge or a curved surface. In rooms where the sound can be defined as almost always diffused, where the surfaces reflections are predominant and the distances between sources and receivers are large, the diffracted contribution in the simulation can be neglected. But within rooms such as open offices where there are surfaces with high absorption coefficients like the ceiling, it can be assumed that diffraction phenomena cannot be neglected and could change noticeably the simulation results, even more if source and receivers are hidden one of each other [25].

The following parts present numeric simulations in an open office model which correspond to a France Telecom call center. Calculations have been made using ICARE and are based on a beam tracing algorithm with the uniform diffraction theory which can model the acoustic field in the shadow area [2], [3], [26]. A comparison with a study made by Peutz & Co. has been made; the results are presented in the following sections.

3.2 Configuration of the two studies

3.2.1 Peutz & Co study

The open plan office studied by Peutz & Co. [27] is a typical call centre with dimensions of 31.5 x 12.8 x 3.1 m^3 and which host around 60 operators. This kind of office is usually subject to a lot of noises because of the numerous noise sources (each operator) which are only separated one from each other only by a screen.

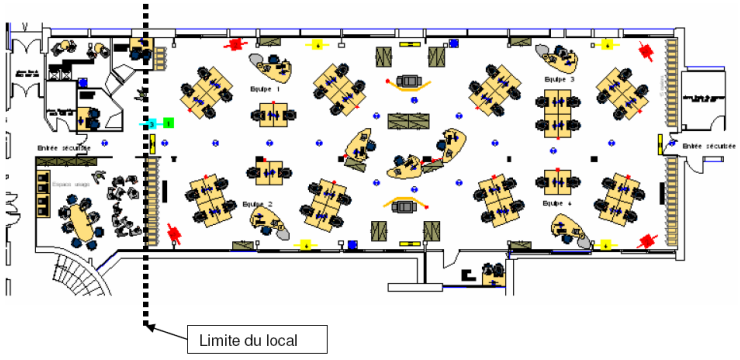

Figure 3-1: 2D view of the open plan office

The study made by Peutz has looked into the reverberation time in the room, the spatial decay and the cartography of the global sound level for different configurations in the room. To make those calculations they use the models presented on Figure 3-2. The tables have been modeled by an equivalent surface with a 0.8 m elevation from the ground.

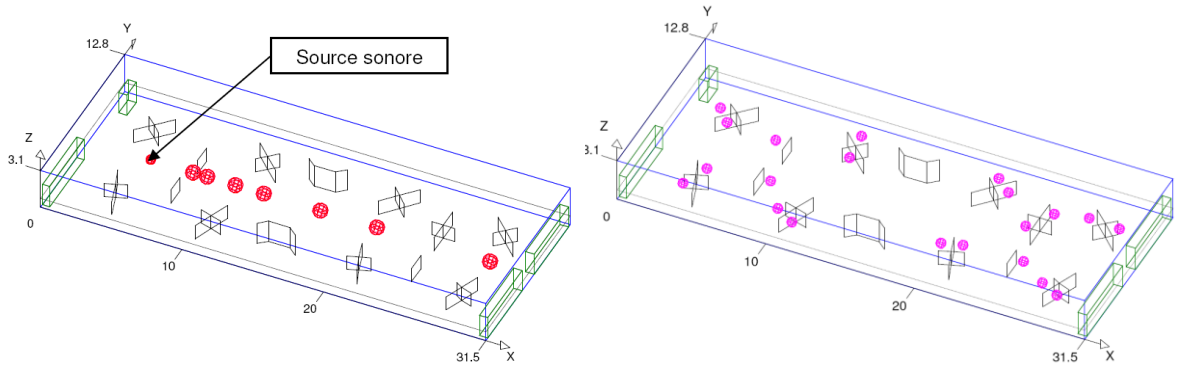

Figure 3-2: 3D model used by Peutz for the spatial decay calculation (left) and for the cartography calculation (right)

The different configurations differ by the height of the screens which varies from 1.10 m to 1.50 m and also the material properties. The sound sources used are unidirectional and their power spectra are defined to match the human voice. The receivers are also unidirectional.

3.2.2 CSTB study

The CSTB study differ from Peutz's one from the 3D model used for the calculations with ICARE. Indeed in CSTB model vertical and horizontal diffraction edges have been defined on every screen separating each operator. Moreover in CSTB model instead of using an equivalent surface to model the tables and the rest of the furniture, every table has been modeled.

The same material properties have been used for our study: the tables, the screens and the walls are purely reflecting whereas the ceiling and the ground have respectively a 0.95 and 0.13 absorption coefficient at 1000 Hz. The sources and the receivers have been chosen unidirectional at the beginning. For the calculation of the spatial decay the source and receivers positions respect the 30th of august 1990 decree relative to the acoustic correction of working spaces [28], see Figure 3-4(a). For the cartography a receiver grid and one source have been used, see Figure 3-4(b), at 1.15 m from the ground to correspond more or less with the height of a sitting person. Also each point of the receiver grid is effectively composed with a sphere of seven receivers, see Figure 3-3, which corresponds to the characteristic dimension of a human head. This receivers sphere is used to solve the problem of pressure modes which leads to pressure variations on small distances. For each

receiver sphere the pressure is calculated at the seven receivers and then the quadratic pressure is taken to make the sound level cartography.

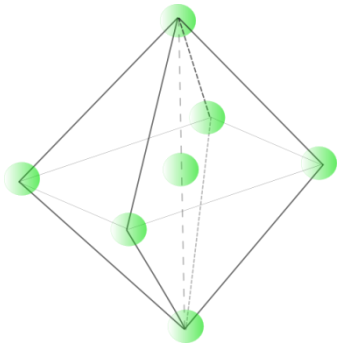

Figure 3-3: the seven receivers which compose a sphere receiver

The aim of the study is to show the influence of taking into account the diffraction phenomena into the simulations that is why it has been decided not to consider the screen height and fixed it at 1.30 m in order for the receivers and the source to be hidden one from each others.

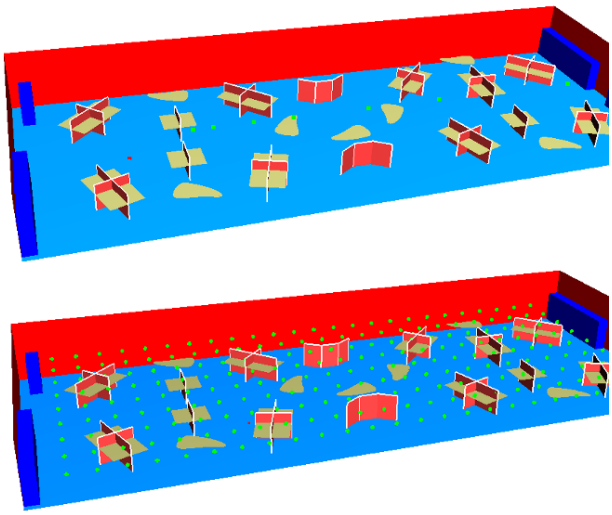

(a)

(b)

Figure 3-4: 3D models used at the CSTB for the spatial decay calculation (a) and for the cartography calculation (b)

3.3 Comparisons of Peutz and CSTB results

3.3.1 Spatial decay DL_2

The Figure 3-5 below introduces the results of the spatial decay DL_2 (linear decay for a doubling distance) obtained by Peutz with their simulation, the pink curve is a regression of the results obtained for each receiver. The green and blue curve corresponds respectively to the regulated spatial decay for an empty office and a full one [28]. One can observe that Peutz model gives a 4.0 dB spatial decay and is a bit below the regulation for an encumbered office which is 3.7 dB for this surface.

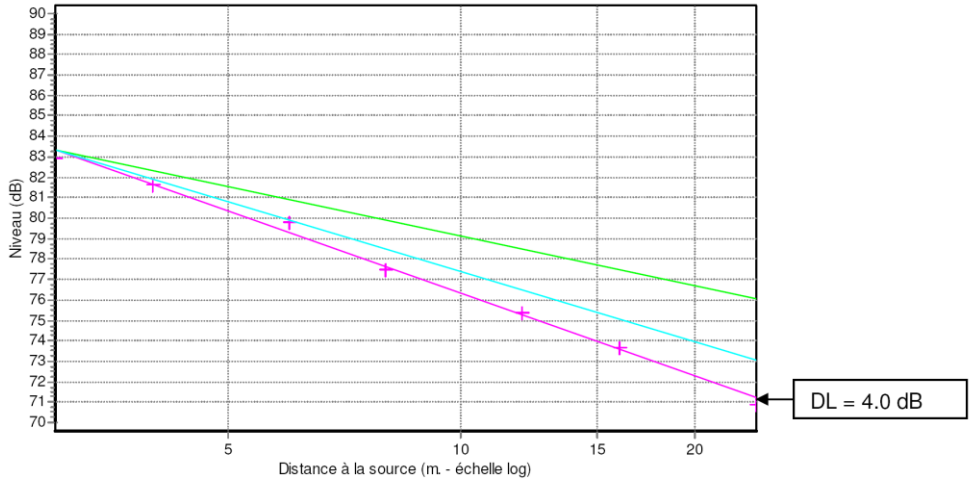

Figure 3-5: Spatial decay calculated by Peutz

The Figure 3-6 below presents the DL_2 values of CSTB model calculated with ICARE. The red and blue curve corresponds respectively to the regression of the results obtained for each receiver without and with diffraction. DL_2 value of 3.02 dB has been obtained for the simulation with diffraction and 2.86 dB for the simulation without diffraction.

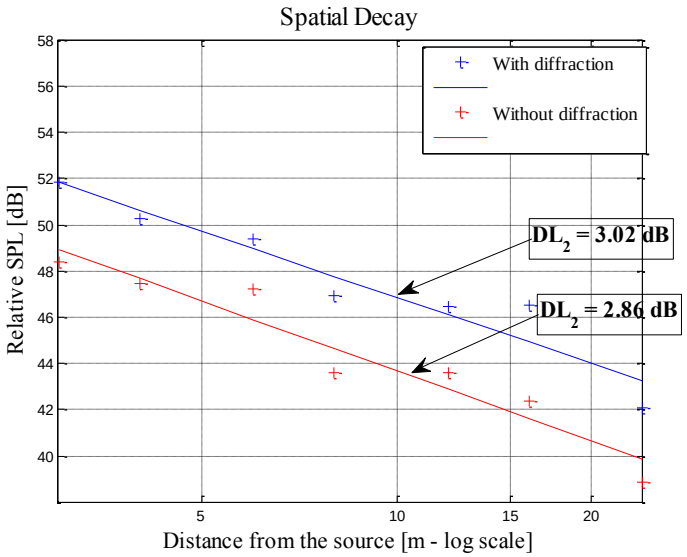

Figure 3-6: Spatial decay calculated at the CSTB with ICARE

3.3.2 Cartography of the mean sound pressure level

The Figure 3-7 below shows a cartography of the mean SPL calculated by Peutz with 21 sources (represented with a pink dot on the figure).

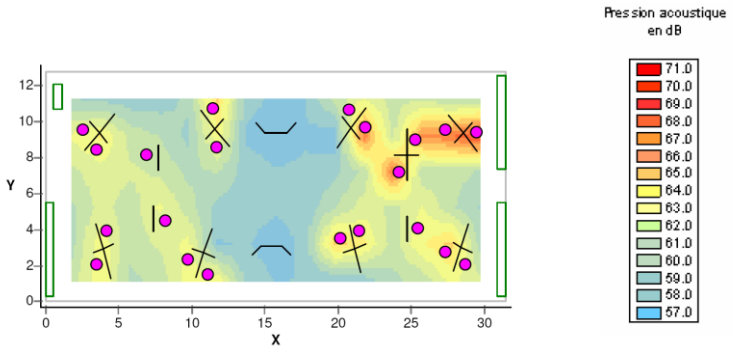

Figure 3-7: Cartography of the mean sound pressure level calculated by Peutz

The Figure 3-8 below shows a cartography of the mean SPL calculated at the CSTB with ICARE. Only one source has been used.

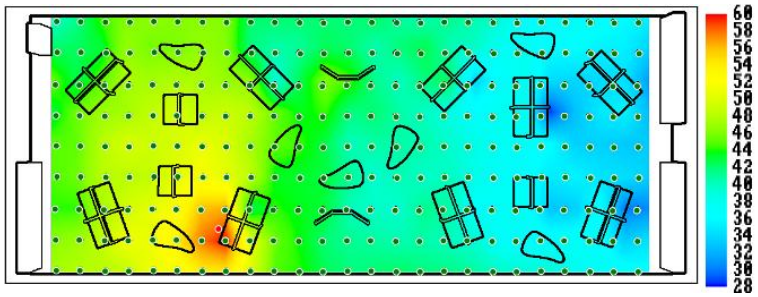

Figure 3-8: Cartography of the mean sound pressure level calculated with ICARE

Since it was complicated to get a similar model than Peutz's one it was even more difficult to get comparative results. That is why the study has only focused on CSTB model to get comparative results with and without diffraction and have a good estimation of the diffraction influence in the simulation.

3.4 CSTB results

Cartography calculations have been made at the CSTB with the ICARE software using a maximum depth of 8 and limiting the number of possible diffraction along a beam path to one. Moreover the propagation depth from each side of diffraction has been limited to 2 at the beginning. The receiver grid was composed of 7*225=1575 receivers and only one source.

On the Figure 3-9 below one can observe the results for the 1000 Hz one-third octave band in relative sound pressure level (SPL) obtained with a unit power source. The Figure 3-9(a) is calculated taking into account the diffraction on the screen edges and the Figure 3-9(b) is calculated without diffraction.

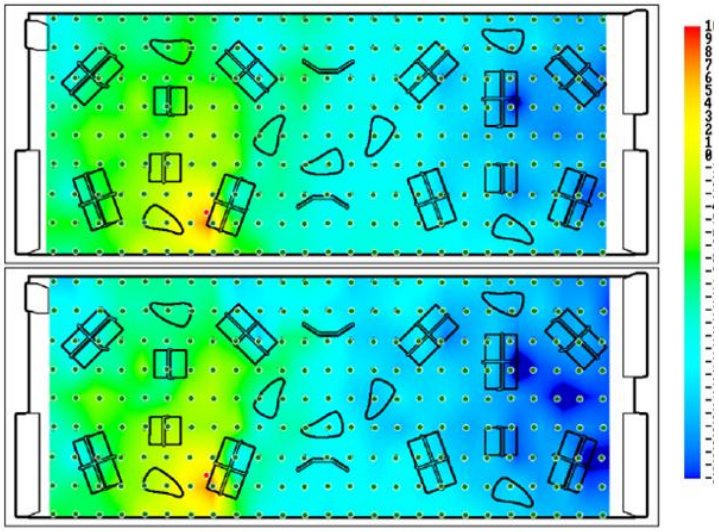

Figure 3-9: Relative sound pressure level calculated with diffraction (a) and without diffraction (b) for the 1000 Hz third octave band

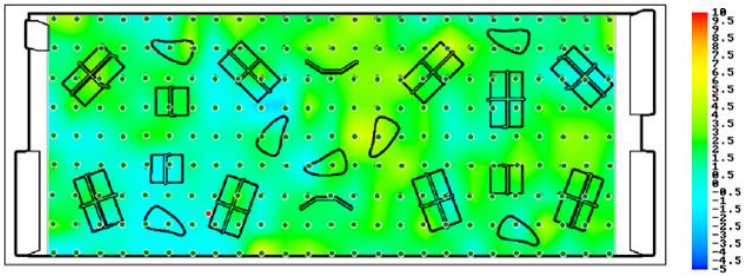

Figure 3-10: Relative sound pressure level difference between calculation with diffraction and without diffraction for the 1000 Hz third octave band

These three figures shows important sound level differences between the calculations made with and without diffraction. Indeed these differences reach 7 dB at some places in the room. Some receivers hidden from the source seem to receive more noise with the inclusion of diffraction in the model. Similar results have been observed on the other one-third octave bands as one can see on the Figure 3-11 for the 500 Hz one-third octave band.

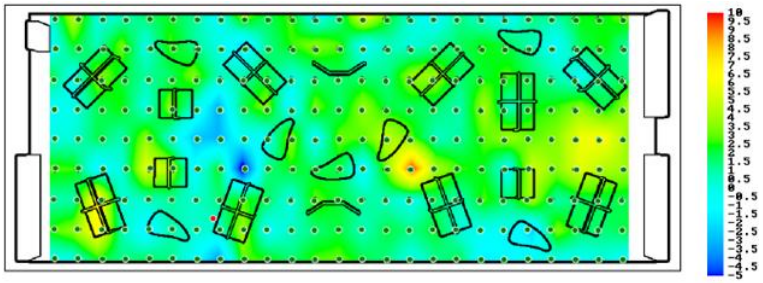

Figure 3-11: Relative sound pressure level difference between calculation with diffraction and without diffraction for the 500 Hz third octave band

3.5 Limitation of the results

3.5.1 Limitation of the propagation depth from each side of the diffraction

The geometric calculation including diffraction, using a beam tracing algorithm, has lasted 33h on an Intel Core 2 Quad 2.66 Ghz, 2.75 Go RAM. Furthermore this calculation has been parallelized in order to use the four different processors in the same time and then decrease the calculation time. Meanwhile the geometric calculation without diffraction has lasted one hour and a half. As it has been said before just one diffraction per propagation path has been authorized and two reflections from each side of this diffraction. However while increasing the propagation depth, the number of diffraction per propagation path or the propagation depth from each side of a diffraction, the calculation time explode substantially. That is why it seems crucial to find criteria for these parameters to insure the correctness of CSTB calculation without having excessive calculation time.

On the Figure 3-12 below one can observe the influence of these parameters on the results. One these figures the calculations have been made with one source (x=42.8m ; y=42m ; z=1.2m) and one receiver (x=55.4m; y=49.1m ; z=1.2m) as it is shown on figure.

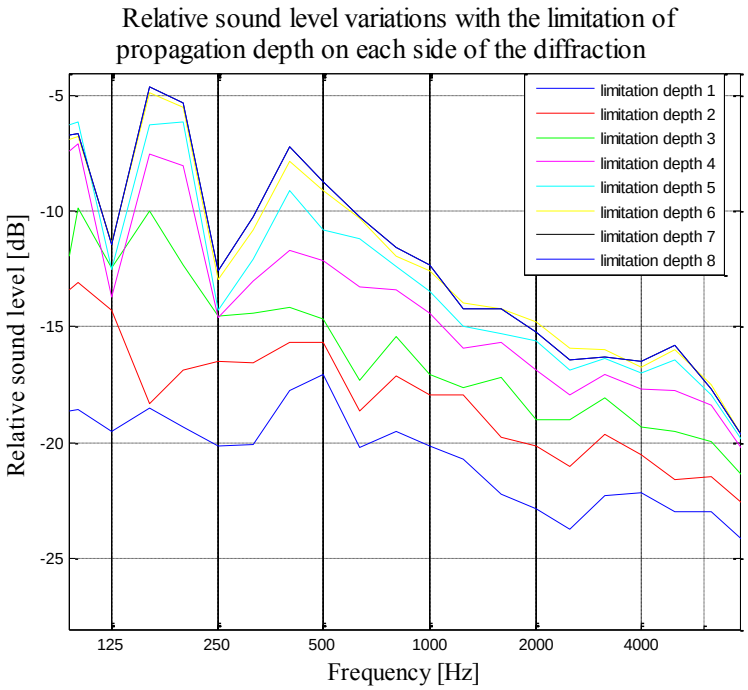

Figure 3-12: Sound pressure level variations with the limitation of the propagation depth from each side of the diffraction

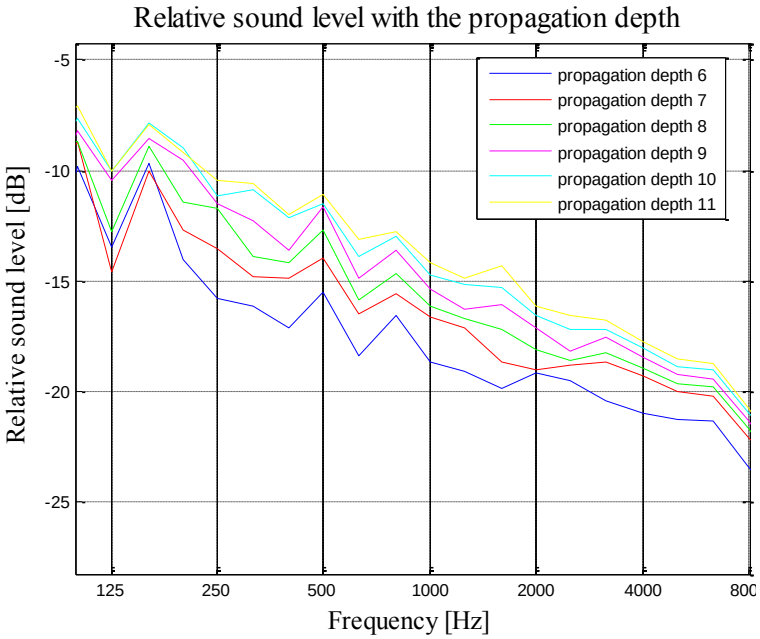

Figure 3-13: Sound pressure level variations with the propagation depth

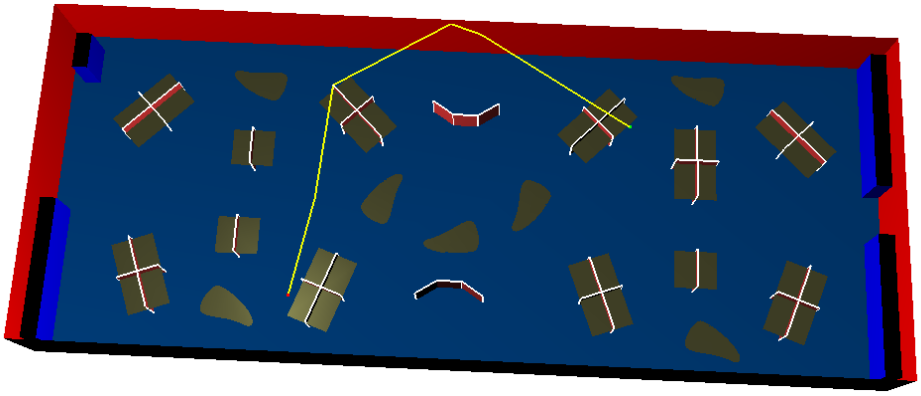

Figure 3-14: example of a diffracted propagation path

From the results on Figure 3-12 and Figure 3-13 one can conclude that the calculation seem to converge for a maximum propagation depth of 8 and for a maximum propagation depth of 5 from each side of the diffraction.

3.5.2 Limitation of the diffraction path in the shadow area

Therefore a solution has been searched to increase the maximum propagation depth from each side of a diffraction but without increasing even more the calculations time.

ICARE already included an option in its diffraction algorithm which was to consider only the path diffracted into the shadow area [29] and don't take into account the diffracted path into the illuminated area. This means that only the

paths which reflection points before and after diffraction don't have a direct sight will be considered. The figure shows the cartographies (in relative SPL) for the 1000 Hz one-third octave band respectively for the calculation with the complete diffraction and for the calculation with the diffraction only in the shadow area. The figure represents relative sound pressure level difference between those two calculations.

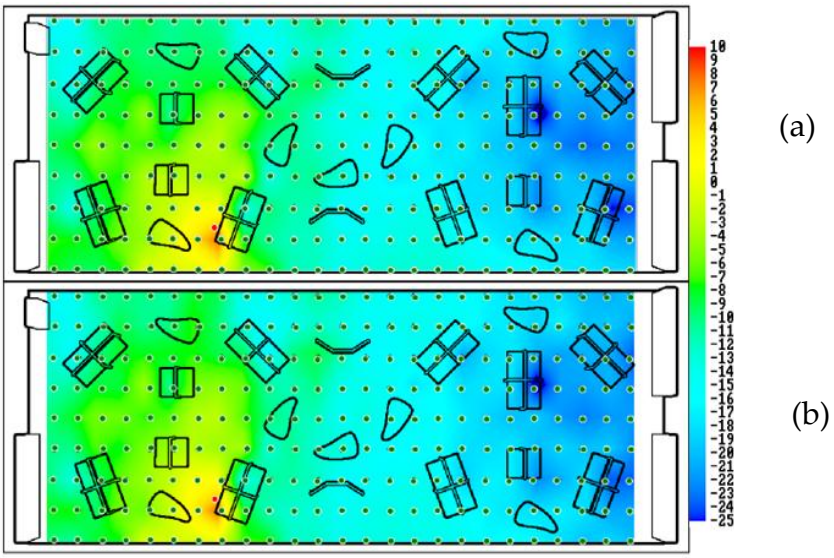

Figure 3-15: Relative sound pressure level calculated with diffraction (a) and without diffraction (b) for the 1000 Hz third octave band

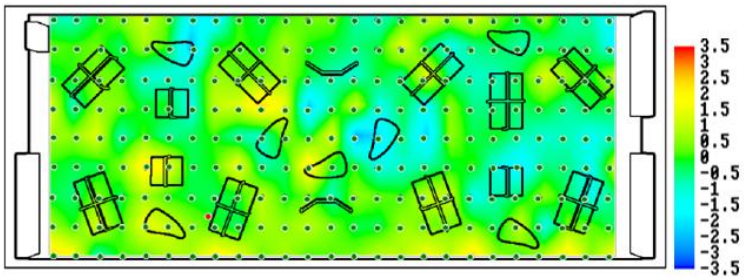

Figure 3-16: Relative sound pressure level difference between calculation with diffraction and without diffraction for the 1000 Hz third octave band

Those figures make us conclude that taking into account the diffraction only in the shadow areas doesn't induce big differences (no more than 2 dB difference). However this conclusion is true for one-third octave bands higher than 800 Hz but for the one-third octave bands between 125 Hz and 600 Hz one can find maximum SPL differences of 4 dB. The figure presents those SPL differences for the 500 Hz one-third octave bands.

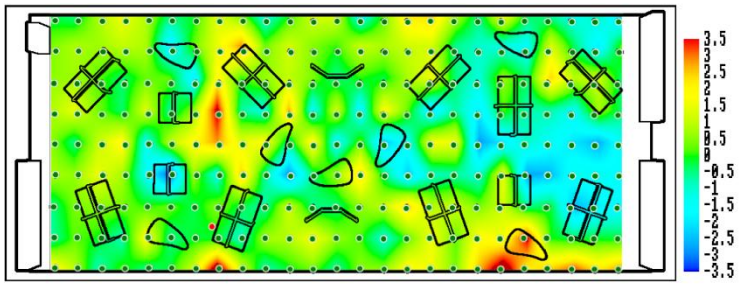

Figure 3-17: Relative SPL difference between calculation with diffraction and without diffraction for the 500 Hz third octave band

The solution which is to limit the diffracted paths only into the shadow areas allows a significant decrease in calculation times. Indeed these calculation times are divided by 4 compared with the calculation described in paragraph 3.5.1. But it is necessary to find out if this solution is sufficient to increase the propagation limitation from each part of diffraction without increasing calculation times. The Figure 3-18 presents relative SPL for different propagation depth limitation from each side of diffraction, as it was shown in Figure 3-12, expect that there is just diffraction into the shadow area here.

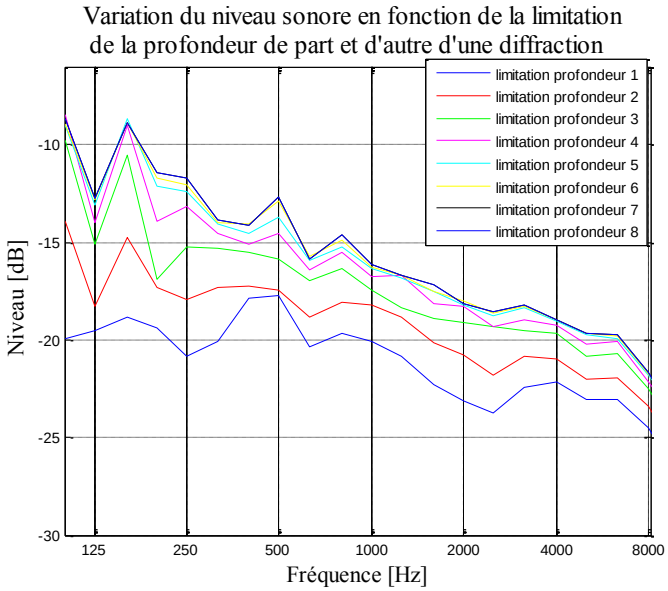

Figure 3-18: SPL variations with the limitation of the propagation depth from each side of the diffraction

With the Figure 3-18 one can see that it is possible to limit the propagation depth from each side of the diffraction to 5 reflections when only diffraction into the shadow area is considered.

The following results present cartographies that have been calculated with diffracted paths only in the shadow areas and higher maximum propagation depth before and after diffraction. In order to make more calculation tests it has

been decided to work on a half size 3D model but the receiver grids stay the same.

The Figure 3-19 shows that the fact to increase the maximum propagation depth before and after diffraction induces an increase of the SPL over the whole room which means that the calculations obtained in part 3.4 haven't converged.

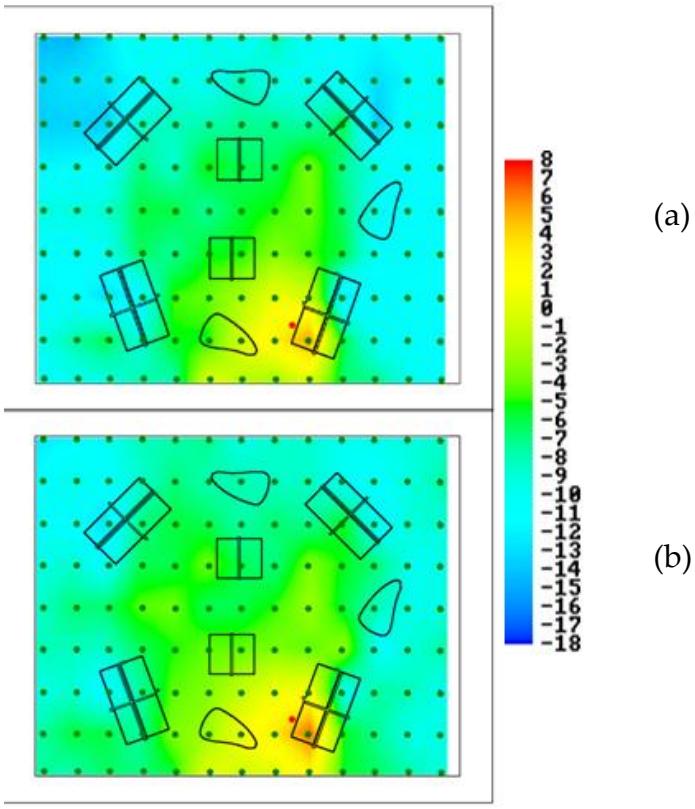

Figure 3-19: Relative sound pressure level at 1000Hz with limitation of the propagation depth from each side of the diffraction of 2 (a) and 4 (b)

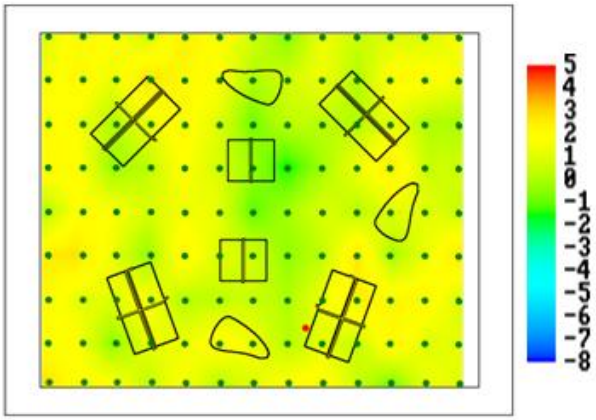

Figure 3-20: Relative sound pressure level difference at 1000Hz between calculations with a limitation of 4 and a limitation of 2

For this half size model the calculations also converge for a propagation depth limitation before and after the diffraction of 6. The following Figure 3-21 shows the relative SPL difference between the calculation using a limitation value of 6 and a limitation value of 4.

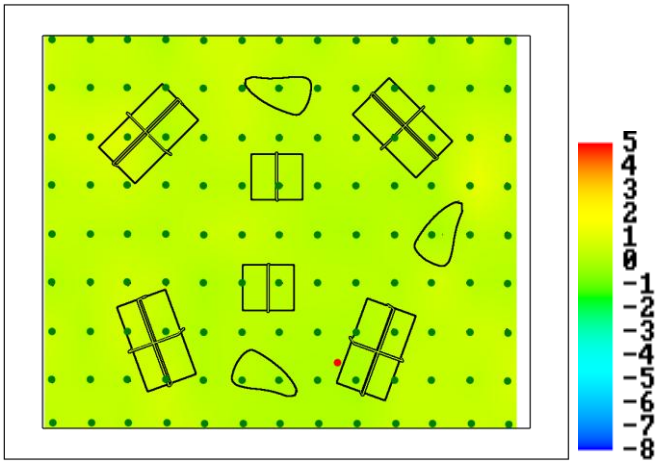

Figure 3-21: Relative sound pressure level difference at 1000Hz between calculations with a limitation of 6 and a limitation of 4

One can see on this figure that with propagation depth on each side of the diffraction of 6 instead of 4 there is a negligible difference whereas the computation time and memory increase significantly.

3.6 Conclusion of this study

This study shows the real interest to take the diffraction phenomena into account in the acoustics simulations even if it is such a time expensive calculation. However, as it has been in previous parts, there are some ways to limit the calculation times but it is necessary to find other ways to increase their precision without increasing calculation times. Another solution to decrease these calculation times would be to make 2.5D calculations; indeed the 3D approach doesn't seem to be adapted for these kind of open plan offices models.

The simulations also proved that a spatial decay calculation is not sufficient to emphasize the differences introduced by the inclusion of diffraction, which can be considered as a really important phenomenon in the open plan offices.

Moreover the solution chosen by Peutz to choose an equivalent surface to model the tables and all the other furniture could be a good alternative compared to the detailed models because it could decrease calculation times without changing the physical properties of the room. But it could also be a risk of decreasing the spatial precision of the sound level.

U.P. Svensson [30] claims that high reflection orders are of limited interest knowing that in realistic situations diffused and diffracted contributions will shadow after few reflection orders. Indeed our calculations only focused on the diffraction influence whereas diffusion and reverberation have been eclipsed on purpose. It would be interesting and more realistic to study the diffraction influence taking the two other phenomena into account.

Another limit that can be seen to this study is that the cartography calculations only used one source whereas a typical open plan office has numerous sources (operators, ventilation systems …). Moreover voices have a peculiar directivity that must be taken into account in order to compare the simulation with measures.

Finally this study has shown quite well the difficulty of including the diffraction into open plan office simulations. Simple calculations as the spatial decay DL_2 are not sufficient for the detailed study of these complex rooms.

4 References

References are given according to the schemes given below for some applications: papers, publications, books and handbooks/codes.

[1] CSTB website, http://international.cstb.fr/default.asp,

Retrieved: October, 2009

[2] N. Noé, F. Gaudaire, M. Vermet: *A general ray-tracing solution to reflection on curved surfaces and diffraction by their bounding edges*. Proceedings of the ICTCA 9th convention, Dresden, Germany, 2009.

[3] N. Noé, F. Gaudaire: *Icare Notice Technique*. CSTB 10th July 2008.

[4] M. Emerti, *Simulation Binaurale de l'acoustique des salles de concert.* PhD thesis, Grenoble Institute of Technology, France, 1995.

[5] Sami Kiminki: *Sound propagation theory for linear ray acoustic modelling*. Helsinki University of Technology Master thesis

[6] Allred, J., Newhouse, A. (1958): *Applications of the Monte Carlo method to architectural acoustics*. J. Acoust. Soc. Am. 30, pp. 1-3.

[7] Allred, J., Newhouse, A. (1958): *Applications of the Monte Carlo method to architectural acoustics. II*," J. Acoust. Soc. Am. 30, pp. 903-904.

[8] M. Pharr, G. Humphreys: *Physically Based Rendering: From Theory to Implementation (The Interactive 3d Technology Series),* Elsevier Inc., 3rd Edition, 2004

[9] N. Noé: *Etude de fonctions de distribution de la réflectance bidirectionnelle*. PhD thesis, University Jean Monnet of Saint Etienne, France, 1999

[10] Z. Xiangyang: *An improved broad-spectrum room acoustics model including diffuse reflections*. Appl. Acoust., Vol. 66, No. 1309–1319, 2005.

[11] T. J. Cox and P. D'Antonio: *Acoustic Absorbers and Diffusers: Theory, Design and Application*. Spon Press, 2nd Edition, 2009.

[12] Kuttruff *H.*: Room *Acoustics: The Fifth Edition*. London: Spon Press, 2009.

[13] M. Vorländer: *Auralization. Fundamentals of Acoustics, Modelling, Simulation, Algorithms and Acoustic Virtual Reality*, Springer, 2008.

[14] Picaud J.: *Application numérique du concept de particules sonores à la modélisation des champs sonores en acoustique architecturales*. Bulletin des Laboratoires des Ponts et Chaussées, Vol. 258-259, pp. 59-88, October-November-December 2005.

[15] J.J. Embrechts: *Broad spectrum diffusion model for room acoustics ray tracing algorithm*. J Acoust. Soc. Am., Vol. 107, pp. 2068–2081, 2000.

[16] S. Lessoine: *Techniques d'accélérations du tir de rayons pour la simulation acoustique*. DEA Thesis, University of Lieges, Belgium, 2006

[17] S. Lessoine: *Size-adaptative spherical receptor acceleration method for acoustical ray-tracing*. Euronoise conference 2008, Paris, France, June 29 - July 4, 2008

[18] B-I. L.Dalenbäck: *Room acoustic prediction based on a unified treatment of diffuse and specular reflection*. J. Acoust. Soc. Am., Vol. 100, pp. 899-909, August 1996

[19] Lam Y.W.: *On the modelling of diffuse reflections in room acoustics prediction*. Refereed Invited Paper, Proc. BEPAC & EPSRC Conference on Sustainable Building, p.106-113, 1997.

[20] Christensen C., Rindel J.: *A new scattering method that combines roughness and diffraction effects*. Forum Acousticum, Budapest, Hungary, 2005

[21] Maercke D, Martin J.: *The prediction of echograms and impulse response within the Epidaure software*. Appl. Acoust., Vol. 38, pp. 93–114, 1993

[22] R. Loyet, J. Maillard, J.C. Iehl, B. Peroche: *Graphe des réflexions dans les volumes complexes* : *construction*, *simplifications perceptives et auralisation*. CFA 2010, Lyon, France, April 2010

[23] I. Bork: *A Report on the 3rd Round Robin on Room Acoustical Computer Simulation*. Acustica - Acta Acustica,Vol. 91, pp. 740 – 752, 2005.

[24] B. Katz: *International Round Robin on Room Acoustical Impulse Response Analysis Software 2004*. J. Acoust. Soc. Am., Vol., No., August 2004.

[25] Christensen C. L.: *Odeon Room Acoustics Program, Version 7.0, "User Manual"*. Industrial,Auditorium and Combined Editions, Odeon A/S, Lyngby, Denmark, 2004.

[26] Deille O., Maillard J., Noé N., Bouatouch K. and Martin J.: *Real Time Acoustic Rendering of Complex Environments Including Diffraction and Curved Surfaces*. Proceedings of the AES 120th convention, Paris, France, 2006.

[27] Chang D., Peutz & Associés : *Centre d'appel France Télécom type. Etude de l'acoustique interne*. AFNOR S30D N518, 2006.

[28] *Arrêté du 30 août 1990 pris pour l'application de l'article R. 235-11 du code du travail et relatif à la correction acoustique des locaux de travail 1990*.

[29] Tsingos N., Funkhouser T., Ngan A., Carlbom I.: *Modeling Acoustics in Virtual Environments Using the Uniform Theory of Diffraction*. Proceedings of the 28th annual conference on Computer graphics and interactive techniques, Los Angeles, California, USA, 2001

[30] Svensson P., Kristiansen U. R.: *Computational Modelling and Simulation of Acoutic Space*. Proceedings of the AES 22nd International Conference on Virtual, Synthetic and Entertainment Audio, Espoo, Finland, 2002.

Appendix A: Definition of the criteria

The **Schroeder's method** is used to find the reverberation time by extrapolation to 60 dB of a line fitted to the reverberation from -5 dB to -35 dB of decay (which corresponds to RT30) or from -5 dB to -25 dB of decay (which corresponds to RT20):

$$RT_{30} = 2\left[t\left(L_p(-35dB)\right) - t\left(L_p(-5dB)\right)\right]$$

$$RT_{20} = 2\left[t\left(L_p(-25dB)\right) - t\left(L_p(-5dB)\right)\right]$$

The **early decay time** (EDT) is the extrapolation to 60 dB of the reverberation time during the first 10 dB of reverberation decay.

Definition is a metric used to judge the suitability of rooms for speech. This metric is made on the assumption that only the 50 first ms of the sound arriving is "useful" in the reverberation process, i.e. beneficial to speech intelligibility.

$$D_{50} = 10log_{10}\frac{\int_0^{50ms} h^2(t)}{\int_0^{\infty} h^2(t)}$$

Where h(t) corresponds to the impulse response.

Clarity, **C** or **C80**, is a metric value similar to Definition but adapted to rooms for music. C80 values indicate how the ratio of early-to-late arriving sound levels varies:

$$C_{80} = 10log_{10}\frac{\int_0^{80ms} h^2(t)}{\int_{80ms}^{\infty} h^2(t)}$$

The **TS** parameter, **Centre Time**, is the time of the centre of gravity of the squared impulse response.

Appendix B: criteria for RR3-phase1 (S1R2)

		Constant radius limited by the geometry	Growing radius limited by the geometry	Growing and truncated radius	RR3 phase 1 - mean value	Standard deviation	Interquartile
125 Hz	TR30	1.89	1.89	1.89	1.88	0.20	0.03
	EDT	1.68	1.64	1.65	1.89	0.31	0.07
	D50	40.31	41.84	39.35	35.00	7.48	2.13
	C80	1.12	1.86	1.36	-0.50	2.16	0.50
	Tc	111.72	107.13	110.63	132.01	44.71	9.07
250 Hz	TR30	1.87	1.87	1.87	1.87	0.18	0.03
	EDT	1.66	1.62	1.63	1.87	0.27	0.06
	D50	40.55	42.07	39.57	35.89	4.99	2.07
	C80	1.16	1.91	1.41	-0.12	0.92	0.30
	Tc	110.69	106.13	109.61	126.52	23.86	10.50
500 Hz	TR30	1.85	1.85	1.85	1.87	0.16	0.06
	EDT	1.63	1.59	1.60	1.82	0.18	0.07
	D50	40.93	42.45	39.94	36.77	4.10	1.00
	C80	1.24	1.99	1.49	0.01	0.82	0.26
	Tc	109.06	104.54	107.99	123.89	19.78	9.82
1000 Hz	TR30	1.81	1.81	1.81	1.83	0.12	0.07
	EDT	1.60	1.55	1.57	1.79	0.19	0.08
	D50	41.45	42.96	40.44	37.65	3.78	3.35
	C80	1.35	2.10	1.60	0.21	0.71	0.21
	Tc	106.90	102.45	105.86	120.88	17.31	8.62

2000 Hz	TR30	1.72	1.72	1.72	1.74	0.11	0.08
	EDT	1.51	1.46	1.48	1.67	0.13	0.15
	D50	42.82	44.29	41.76	39.03	3.62	3.80
	C80	1.63	2.39	1.88	0.51	0.63	0.50
	Tc	101.53	97.25	100.55	113.57	13.99	9.78
4000 Hz	TR30	1.44	1.44	1.44	1.48	0.12	0.09
	EDT	1.24	1.19	1.22	1.43	0.12	0.15
	D50	47.61	48.95	46.39	43.70	3.40	3.27
	C80	2.60	3.40	2.87	1.46	0.64	0.70
	Tc	85.54	81.85	84.78	96.33	14.16	10.30

Appendix C: convergence calculation

Convergence calculations on RT30, EDT, D50 and Ts when N_{spec} is changing, see Part 2.5.

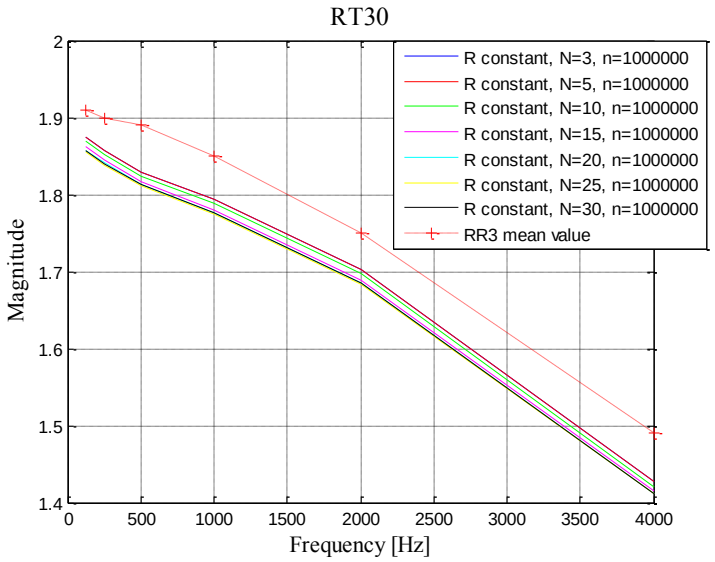

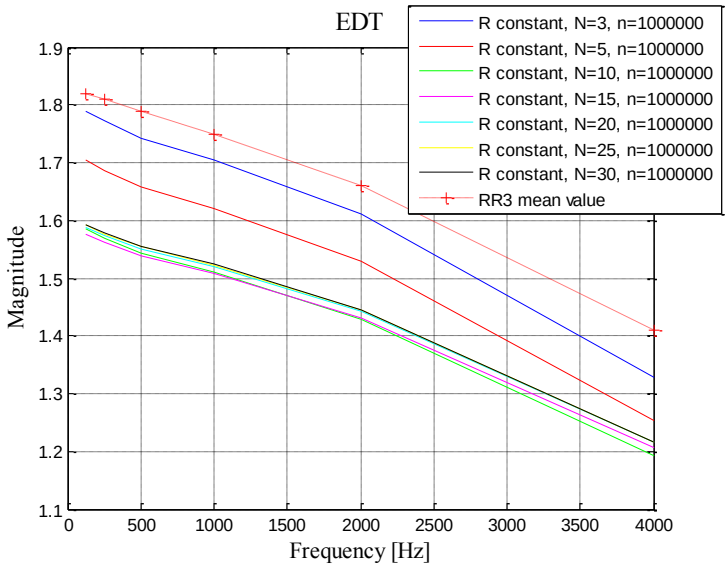

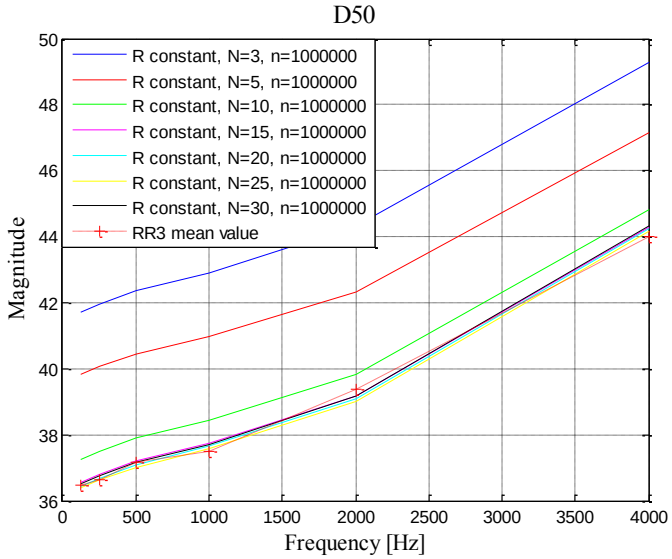
D50
R constant, N=3, n=1000000
R constant, N=5, n=1000000
R constant, N=10, n=1000000
R constant, N=15, n=1000000
R constant, N=20, n=1000000
R constant, N=25, n=1000000
R constant, N=30, n=1000000
RR3 mean value
Magnitude
Frequency [Hz]

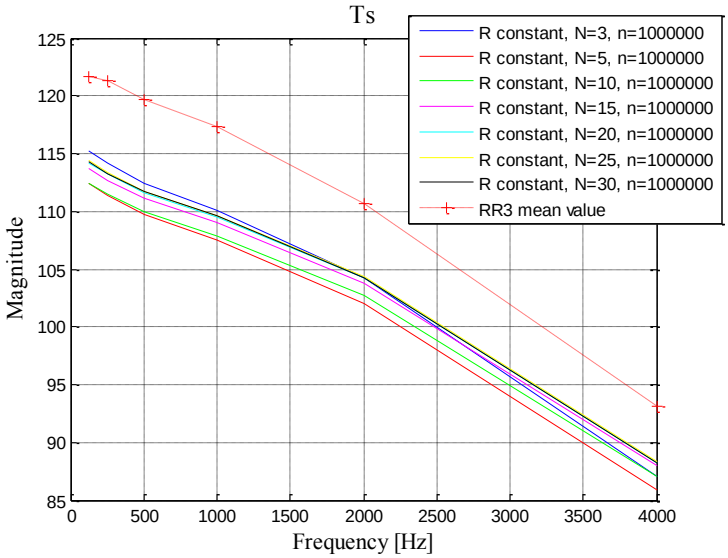
Ts
R constant, N=3, n=1000000
R constant, N=5, n=1000000
R constant, N=10, n=1000000
R constant, N=15, n=1000000
R constant, N=20, n=1000000
R constant, N=25, n=1000000
R constant, N=30, n=1000000
RR3 mean value
Magnitude
Frequency [Hz]

Appendix D: Criteria and comparison with RR3 phase1 and phase2 results

All the criteria presented in this appendix are the mean criteria values for all the combinations source/receiver.

- **Criteria with RR3 phase1 model**

The red curve is the result obtained with ICARE's new algorithm and the blue curve is the mean result of all the users who have participated to the RR3 test. The errors bars present the standard deviation of all the participant's results.

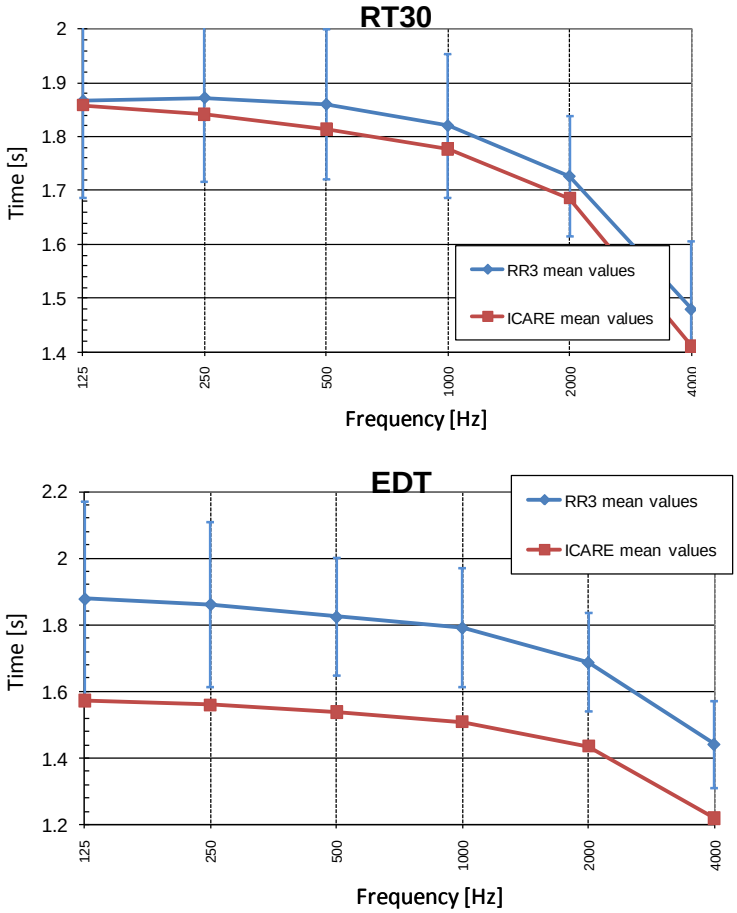

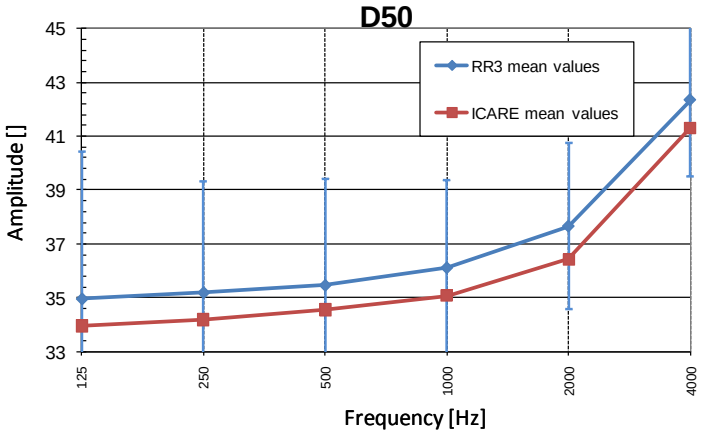

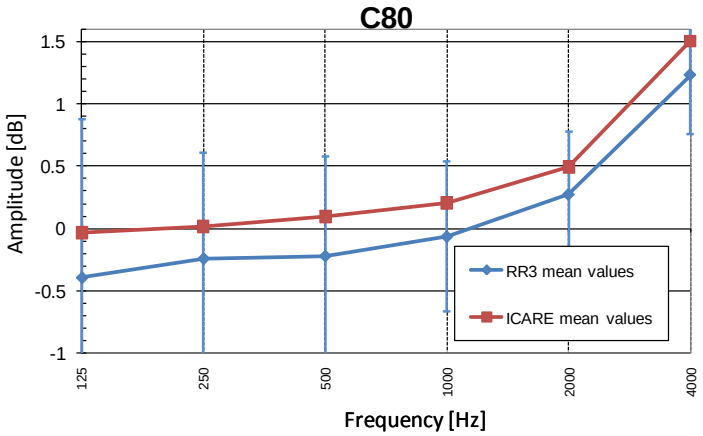

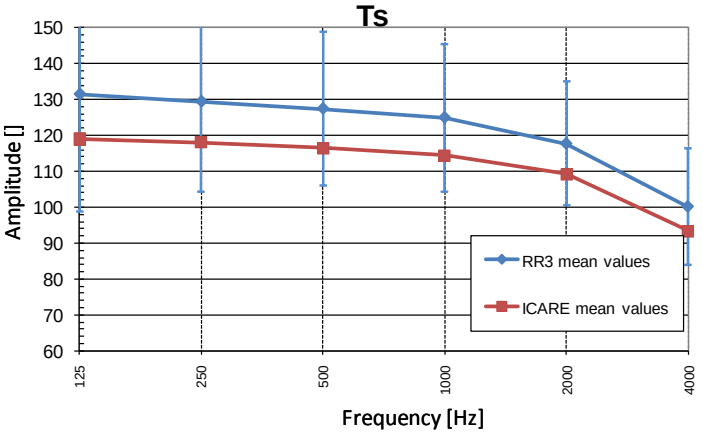

- **Criteria with RR3 phase2 model**

The red curve is the result obtained with ICARE's new algorithm, the green curve is the results of the measurement and the blue curve is the mean result of all the users who have participated to the RR3 test.

The errors bars present the standard deviation of all the measures results.

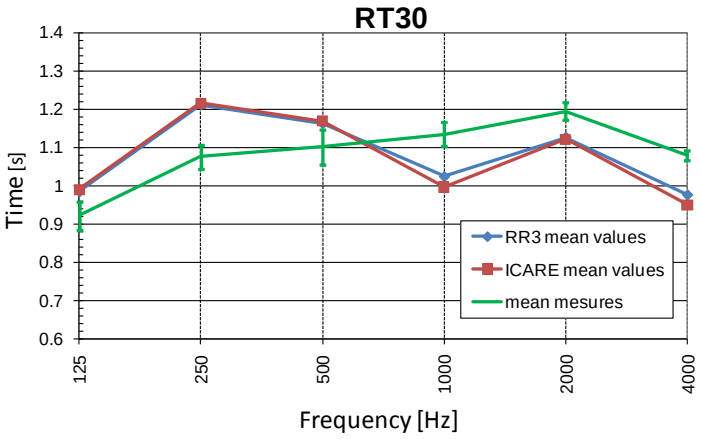
RT30
Time [s]
1.4
1.3
1.2
1.1
1
0.9
0.8
0.7
0.6
125
250
500
1000
2000
4000
Frequency [Hz]
RR3 mean values
ICARE mean values
mean mesures

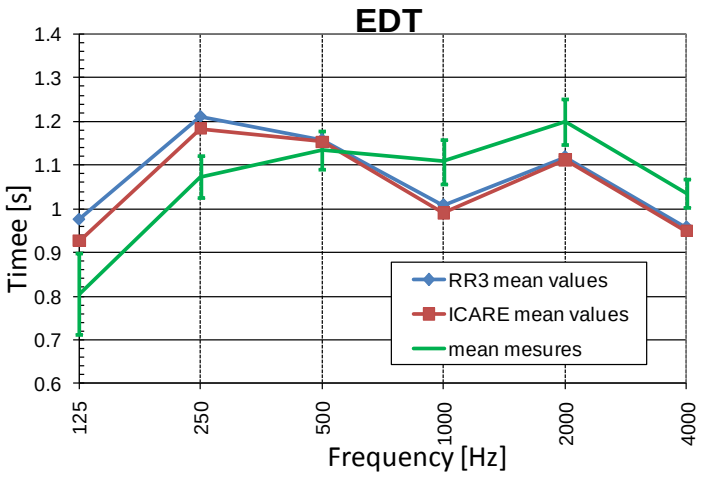
EDT
Timee [s]
1.4
1.3
1.2
1.1
1
0.9
0.8
0.7
0.6
125
250
500
1000
2000
4000
Frequency [Hz]
RR3 mean values
ICARE mean values
mean mesures

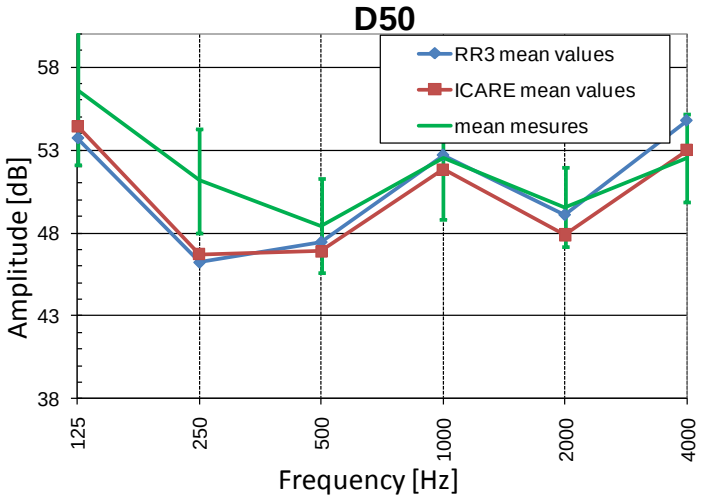
D50
Amplitude [dB]
58
53
48
43
38
125
250
500
1000
2000
4000
Frequency [Hz]
RR3 mean values
ICARE mean values
mean mesures

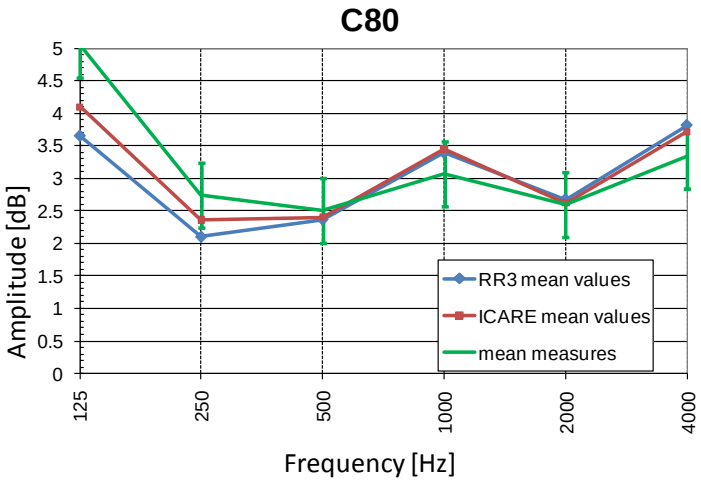
C80
Amplitude [dB]
5
4.5
4
3.5
3
2.5
2
1.5
1
0.5
0
125
250
500
1000
2000
4000
Frequency [Hz]
RR3 mean values
ICARE mean values
mean measures

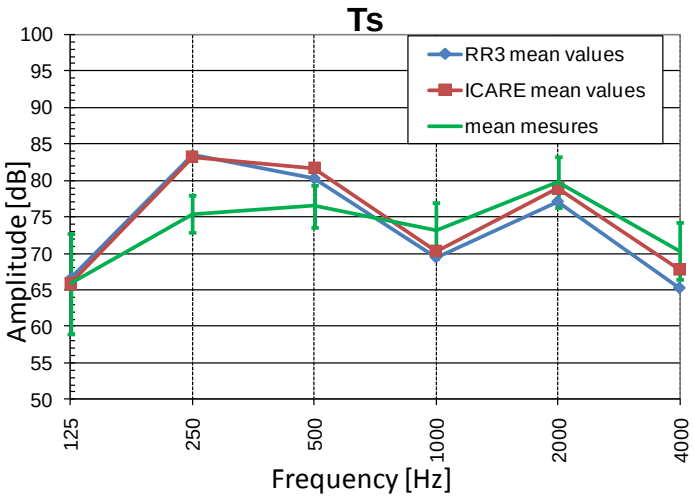
Ts
Amplitude [dB]
100
95
90
85
80
75
70
65
60
55
50
125
250
500
1000
2000
4000
Frequency [Hz]
RR3 mean values
ICARE mean values
mean mesures

Appendix E: ICARE output (impulse response)

Here is presented the impulse response file obtained as an output with ICARE.

: means "comment" and the heading presents the source position, the receptor position and the octave band for which the calculation has been made.

First column: time vector

Second column: absolute values of pressure for the corresponding time value

Third: decay values for the corresponding time value

```
#
# t
# s +1.500000000000 +3.500000000000 +1.500000000000
# t
# r +2.000000000000 +6.000000000000 +1.200000000000
# f +500.000000000000
#
+0.000000000000 +0.000000000000 +2.027444209999
+0.000058274936 +0.000000000000 +2.027444209999
+0.000116549873 +0.000000000000 +2.027444209999
+0.000174824809 +0.000000000000 +2.027444209999
+0.000233099746 +0.000000000000 +2.027444209999
+0.000291374682 +0.000000000000 +2.027444209999
+0.000349649619 +0.000000000000 +2.027444209999
+0.000407924555 +0.000000000000 +2.027444209999
+0.000466199492 +0.000000000000 +2.027444209999
+0.000524474428 +0.000000000000 +2.027444209999
+0.000582749364 +0.000000000000 +2.027444209999
+0.000641024301 +0.000000000000 +2.027444209999
+0.000699299237 +0.000000000000 +2.027444209999
+0.000757574174 +0.000000000000 +2.027444209999
+0.000815849110 +0.000000000000 +2.027444209999
+0.000874124047 +0.000000000000 +2.027444209999
+0.000932398983 +0.000000000000 +2.027444209999
+0.000990673920 +0.000000000000 +2.027444209999
+0.001048948856 +0.000000000000 +2.027444209999
+0.001107223792 +0.000000000000 +2.027444209999
+0.001165498729 +0.000000000000 +2.027444209999
+0.001223773665 +0.000000000000 +2.027444209999
+0.001282048602 +0.000000000000 +2.027444209999
+0.001340323538 +0.000000000000 +2.027444209999
+0.001398598475 +0.000000000000 +2.027444209999
+0.001456873411 +0.000000000000 +2.027444209999
+0.001515148348 +0.000000000000 +2.027444209999
+0.001573423284 +0.000000000000 +2.027444209999
+0.001631698220 +0.000000000000 +2.027444209999
+0.001689973157 +0.000000000000 +2.027444209999
+0.001748248093 +0.000000000000 +2.027444209999
+0.001806523030 +0.000000000000 +2.027444209999
+0.001864797966 +0.000000000000 +2.027444209999
…
```

Appendix F: Case of an infinite diffusing plate

As it is done in the part 2.2 of the report, the quantity of energy emitted by the source which will be received by a collecting sphere – which centre is the receiver point - is the sum of the energy of the particles going directly in the sphere ($|p|^2_{direct}$), the particles being specularly reflected on the plate ($|p|^2_{specular}$) and the particles being diffusively reflected on the plate ($|p|^2_{diffuse}$).

$$|p|^2_{received} = |p|^2_{direct} + |p|^2_{specular} + |p|^2_{diffuse}$$

Knowing that the energy can be expressed using the power density dW as it expressed in the following equation:

$$|p|^2 = \rho c \frac{dW}{dS}$$

ρ is the density of the air and c the speed of sound.

Then the energy of the particles going directly at the receiver is:

$$|p|^2_{direct} = \rho c \frac{W_0}{4\pi r_d^2}$$

W_0 is the power of the source and r_d is the distance between the source and the receiver.

The energy of the particles being specularly reflected on the plate is:

$$|p|^2_{specular} = (1-\alpha)(1-\delta)\rho c \frac{W_0}{4\pi r_s^2}$$

r_s is the distance covered during the specular reflection, α is the absorption coefficient and δ is the diffusion coefficient.

The energy of the particles being diffusively reflected on the plate is:

$$|p|^2_{diffuse} = \delta(1-\alpha)\rho c W_0 n_{sphere,diffused}$$

Where $n_{sphere,diffused}$ is the number of particles arriving in the collecting sphere, which centre is the receiver. This number can be expressed, as it has been done in § 2.2.4 of the thesis report.

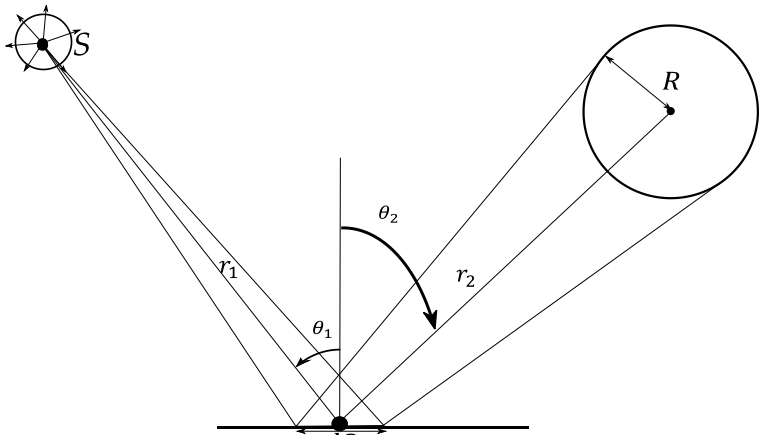

In the figure above, the number of particles $dn_{incident}$ emitted by a spherical source and arriving on a surface element dA can be formulated with the following equation:

$$dn_{incident} = \frac{dAcos\theta_1}{\pi r_1^2} \times n_{source}$$

Where θ_1 is the angle between the normal of the surface and the trajectory of the incident particle; $r_1$is the distance between the source and the reflexion point. θ_2 is the angle between the normal of the surface and the trajectory of the reflected particle and r_2 is the distance between the reflexion point and the centre of the collecting sphere, i.e. the position of the receiver.

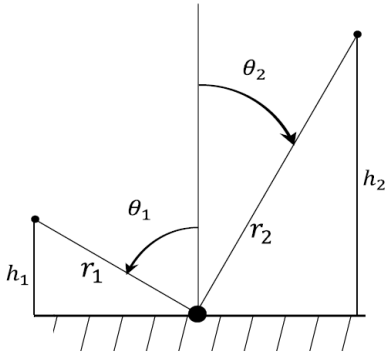

The number of diffused particles $n_{sphere,diffused}$ received by the sphere is equivalent to the sum on the surface dA of the punctual diffuse reflection described, thus $n_{sphere,diffused}$ can be expressed by:

$$n_{sphere,diffused} = \int dn_{incident} \frac{R^2 cos\theta_2}{r_2^2} = R^2\, n_{source} \int \frac{cos\theta_1 cos\theta_2 dA}{\pi r_1^2 r_2^2}$$

Finally the energy of the particles being diffusively reflected on the plate is:

$$|p|^2_{diffuse} = (1-\alpha)\delta\rho c W_0 \int dn_{incident} \frac{R^2 cos\theta_2}{r_2^2}$$
$$= (1-\alpha)\delta\rho c W_0 R^2\, n_{source} \int \frac{cos\theta_1 cos\theta_2 dA}{\pi r_1^2 r_2^2}$$

Which give the following expression for the energy received by the collecting sphere:

$$|p|^2_{received} = \rho c \frac{W_0}{4\pi}\left(\frac{1}{r_d^2} + (1-\alpha)(1-\delta)\frac{1}{r_s^2} + (1-\alpha)R^2\, n_{source} \int \frac{cos\theta_1 cos\theta_2 dA}{\pi r_1^2 r_2^2}\right)$$

Then if one considers a point to point path from the source to the receiver it is possible to get the following formula:

$$|p|^2_{received} = \rho c \frac{W_0}{4\pi}\left(\frac{1}{r_d^2} + (1-\alpha)(1-\delta)\frac{1}{r_s^2} + (1-\alpha) \int \frac{cos\theta_1 cos\theta_2 dA}{\pi r_1^2 r_2^2}\right)$$

In this expression the integral does not have any analytical solution but it is possible to compute it in an algorithm.

As it is done in the part 2.2 of the report, the quantity of energy emitted by the source which will be received by a collecting sphere – which centre is the receiver point - is the sum of the energy of the particles going directly in the sphere ($|p|^2_{direct}$), the particles being specularly reflected on the plate ($|p|^2_{specular}$) and the particles being diffusively reflected on the plate ($|p|^2_{diffuse}$).